

การวิเคราะห์หน่วยแรงที่สำหรับรอยร้าวในตัวกลางไฟอโซอีเล็กทริกเชิงเส้น 3 มิติ



นายไตรภพ ทรัพย์สถาผล

จุฬาลงกรณ์มหาวิทยาลัย

CHULALONGKORN UNIVERSITY

วิทยานิพนธ์นี้เป็นส่วนหนึ่งของการศึกษาตามหลักสูตรปริญญาวิศวกรรมศาสตรมหาบัณฑิต

สาขาวิชาวิศวกรรมโยธา ภาควิชาวิศวกรรมโยธา

คณะวิศวกรรมศาสตร์ จุฬาลงกรณ์มหาวิทยาลัย

ปีการศึกษา 2556


ลิขสิทธิ์ของจุฬาลงกรณ์มหาวิทยาลัย

บทคัดย่อและแฟ้มข้อมูลฉบับเต็มของวิทยานิพนธ์ตั้งแต่ปีการศึกษา 2554 ที่ให้บริการในคลังปัญญาจุฬาฯ (CUIR)

เป็นแฟ้มข้อมูลของนิสิตเจ้าของวิทยานิพนธ์ ที่ส่งผ่านทางบัณฑิตวิทยาลัย

The abstract and full text of theses from the academic year 2011 in Chulalongkorn University Intellectual Repository (CUIR) are the thesis authors' files submitted through the University Graduate School.

ANALYSIS OF T-STRESS FOR CRACKS IN 3D LINEAR PIEZOELECTRIC MEDIA



Mr. Tripop Subsathaphol

จุฬาลงกรณ์มหาวิทยาลัย

CHULALONGKORN UNIVERSITY

A Thesis Submitted in Partial Fulfillment of the Requirements
for the Degree of Master of Engineering Program in Civil Engineering

Department of Civil Engineering

Faculty of Engineering

Chulalongkorn University

Academic Year 2013

Copyright of Chulalongkorn University

Thesis Title	ANALYSIS OF T-STRESS FOR CRACKS IN 3D LINEAR PIEZOELECTRIC MEDIA
By	Mr. Tripop Subsathaphol
Field of Study	Civil Engineering
Thesis Advisor	Associate Professor Jaroon Rungamornrat, Ph.D.
Thesis Co-Advisor	Weeraporn Phongtinnaboot, Ph.D.

Accepted by the Faculty of Engineering, Chulalongkorn University in Partial
Fulfillment of the Requirements for the Master's Degree

.....Dean of the Faculty of Engineering
(Professor Bundhit Eua-arporn, Ph.D.)

THESIS COMMITTEE

.....Chairman
(Professor Teerapong Senjuntichai, Ph.D.)

.....Thesis Advisor
(Associate Professor Jaroon Rungamornrat, Ph.D.)

.....Thesis Co-Advisor
(Weeraporn Phongtinnaboot, Ph.D.)

.....Examiner
(Associate Professor Akhrawat Lenwari, Ph.D.)

.....External Examiner
(Assistant Professor Sasikorn Leungvichcharoen, Ph.D.)

ไตรภพ ทรัพย์สถาผล : การวิเคราะห์หน่วยแรงที่สำหรับรอยร้าวในตัวกลางไพเอโซอิเล็กทริกเชิงเส้น 3 มิติ. (ANALYSIS OF T-STRESS FOR CRACKS IN 3D LINEAR PIEZOELECTRIC MEDIA) อ.ที่ปรึกษาวิทยานิพนธ์หลัก: รศ. ดร.จรรยา รุ่งอมรรัตน์, อ.ที่ปรึกษาวิทยานิพนธ์ร่วม: ดร.วีรพร พงศ์ติณบุตร, 51 หน้า.

วิทยานิพนธ์ฉบับนี้ได้นำเสนอระเบียบวิธีคำนวณเชิงตัวเลขที่มีประสิทธิภาพและมีความถูกต้องแม่นยำสำหรับคำนวณค่าหน่วยแรงที่ทั่วไปของรอยร้าวภายใต้เงื่อนไขขอบเขตเชิงไฟฟ้าแบบไม่ยินยอมให้ประจุไฟฟ้าไหลผ่านในตัวกลางไพเอโซอิเล็กทริกเชิงเส้น 3 มิติไร้ขอบเขตระเบียบวิธีบาวดารีเอเลเมนต์แบบสมมาตรกัลเลอร์คินซึ่งมีสมการกำกับเป็นสมการเชิงปริพันธ์พื้นผิวของปริมาณแรงจุดลากทั่วไปแบบเอกฐานต่ำได้ถูกนำมาใช้ในการคำนวณค่าผลต่างของการกระจัดทั่วไประหว่างผิวบนและล่างของรอยร้าว จากนั้นนำค่าที่คำนวณได้มาใช้ร่วมกับสมการกำกับเชิงปริพันธ์พื้นผิวของปริมาณการกระจัดทั่วไปแบบเอกฐานต่ำ เพื่อคำนวณหาผลรวมของการกระจัดทั่วไประหว่างผิวบนและล่างของรอยร้าว ข้อมูลที่ได้ดังกล่าวนำมาใช้ในการคำนวณค่าหน่วยแรงที่ทั่วไปที่จุดใดๆบนขอบรอยร้าว การใช้สมการเชิงปริพันธ์พื้นผิวแบบเอกฐานต่ำเป็นสมการกำกับทำให้สามารถเลือกใช้ฟังก์ชันพื้นฐานแบบต่อเนื่องในการประมาณค่าของตัวแปรไม่ทราบค่าหลัก และยังช่วยลดความยุ่งยากในการหาค่าปริพันธ์เชิงตัวเลขของปริมาณปริพันธ์แบบเอกฐานที่เกี่ยวข้องทั้งหมดด้วย นอกจากนี้ได้นำฟังก์ชันพื้นฐานแบบพิเศษมาใช้ที่บริเวณขอบรอยร้าวเพื่อให้สามารถจำลองพฤติกรรมของปริมาณสนามบริเวณใกล้ขอบรอยร้าวได้อย่างถูกต้องและลดความต้องการโครงตาข่ายละเอียด ผลจากการวิเคราะห์เชิงตัวเลขสำหรับปัญหาออยร้าวรูปแบบต่างๆ นอกจากพิสูจน์ความถูกต้องของระเบียบวิธีเชิงตัวเลขที่พัฒนาขึ้นแล้ว ยังแสดงถึงความสามารถของระเบียบวิธีดังกล่าวในการวิเคราะห์ปัญหาออยร้าวทั่วไปอีกด้วย



จุฬาลงกรณ์มหาวิทยาลัย
CHULALONGKORN UNIVERSITY

ภาควิชา วิศวกรรมโยธา

สาขาวิชา วิศวกรรมโยธา

ปีการศึกษา 2556

ลายมือชื่อนิสิต

ลายมือชื่อ อ.ที่ปรึกษาวิทยานิพนธ์หลัก

ลายมือชื่อ อ.ที่ปรึกษาวิทยานิพนธ์ร่วม

5570202821 : MAJOR CIVIL ENGINEERING

KEYWORDS: GENERALIZED T-STRESSES / IMPERMEABLE CRACKS / LINEAR
PIEZOELECTRIC MEDIUM / SGBEM / BOUNDARY INTEGRAL EQUATIONS / WEAKLY
SINGULAR / CRACK FRONT

TRIPOP SUBSATHAPHOL: ANALYSIS OF T-STRESS FOR CRACKS IN 3D
LINEAR PIEZOELECTRIC MEDIA. ADVISOR: ASSOC. PROF. JAROON
RUNGAMORN RAT, Ph.D., CO-ADVISOR: WEERAPORN PHONGTINNABOOT,
Ph.D., 51 pp.

This thesis aims to present an accurate and efficient computational scheme for determining the generalized T-stresses of impermeable cracks in a three-dimensional linear piezoelectric infinite medium. A symmetric Galerkin boundary element method (SGBEM), based principally on a weakly-singular generalized traction boundary integral equation, is developed to determine the relative crack-face generalized displacement. Such computed information is then utilized along with the generalized displacement boundary integral equation to obtain the sum of the crack-face generalized displacement. This obtained essential data is then post-processed to extract the generalized T-stresses at any point along the crack front. Use of completely regularized boundary integral equations in the formulation allows the primary unknowns to be approximated by continuous basis functions and, additionally, eases the numerical integration of all involved singular integrals. To further improve the approximation of the near-tip field and lessen the requirement of using fine meshes, special basis functions are utilized in a region adjacent the crack boundary. Extensive numerical experiments for various scenarios are considered and results for certain cases are compared with reference solutions not only to verify the formulation but also to show the ability of the present technique to solve general crack problems.

Department: Civil Engineering

Student's Signature

Field of Study: Civil Engineering

Advisor's Signature

Academic Year: 2013

Co-Advisor's Signature

ACKNOWLEDGEMENTS

I would like to show my great gratitude to my advisor, Associate Professor Dr. Jaron Rungamornrat, and my co-advisor, Dr. Weeraporn Phongtinnaboot, for their kindly support and advices throughout the course of this investigation. I would like to express my sincere thanks to my parents and family who always encourage, support and give me a great opportunity to pursue this graduate study. Last but not least, I would also like to thank all of my friends, faculty administrators, and everyone who helps me to complete this research.



CONTENTS

	Page
THAI ABSTRACT.....	v
ENGLISH ABSTRACT.....	vi
ACKNOWLEDGEMENTS	vi
CONTENTS.....	vii
LIST OF TABLES	ix
LIST OF FIGURE.....	x
LIST OF ABBREVIATIONS	xiii
CHAPTER 1 INTRODUCTION	1
1.1 GENERAL	1
1.2 BACKGROUND AND REVIEW	3
1.2.1 Analysis for Intensity Factors in Piezoelectric Materials	3
1.2.2 T-Stress in Piezoelectric Materials	6
1.3 OBJECTIVES	8
1.4 SCOPE OF RESEARCH.....	8
1.5 METHODOLOGY AND PROCEDURE.....	8
1.6 RESEARCH SIGNIFICANCE.....	9
CHAPTER 2 PROBLEM FORMULATION.....	10
2.1 BASIC EQUATIONS FOR LINEAR PIEZOELECTRICITY	10
2.2 PROBLEM DESCRIPTION.....	11
2.3 TREATMENT OF REMOTE CONDITION	12
2.4 STANDARD INTEGRAL RELATIONS	13
2.5 REGULARIZED INTEGRAL RELATIONS/EQUATIONS	15
CHAPTER 3 DEVELOPMENT OF WEAKLY SINGULAR SGBEM	18
3.1 SOLUTION METHODOLOGY	18
3.2 DISCRETIZATION.....	19
3.3 NUMERICAL INTEGRATION SCHEME	20
3.4 EFFICIENT EVALUATION OF KERNELS.....	20

	Page
3.5	CALCULATION OF GENERALIZED T-STRESS21
CHAPTER 4	NUMERICAL RESULTS AND DISCUSSIONS23
4.1	VERIFICATIONS24
4.1.1	Piezoelectric material.....25
4.1.2	Isotropic and transversely isotropic material.....26
4.2	MORE COMPLEX BOUNDARY VALUE PROBLEMS.....27
4.2.1	Tunnel crack27
4.2.2	Spherical cap crack.....32
4.2.2.1	Uniform remote tension.....33
4.2.2.2	Uniform remote biaxial tension33
4.2.2.3	Uniform remote tension and surface electric charge35
4.2.3	Pair of penny-shaped cracks.....38
CHAPTER 5	CONCLUSIONS AND REMARKS.....44
REFERENCES.....	46
APPENDIX	50
VITA	51

LIST OF TABLES

	Page
Table 4.1 Generalized moduli of PZT-4 and PZT-5H (e.g., Li <i>et al.</i> , 2013; Rungamornrat and Mear, 2008c). The plan of isotropy is taken normal to the x_3 -axis.	23
Table 4.2 Normalized generalized T-stress T_{11} for penny-shaped crack contained in piezoelectric unbounded medium under two loading cases.....	25
Table 4.3 Normalized generalized T-stress T_{33} for penny-shaped crack contained in piezoelectric unbounded medium under two loading cases.....	25
Table 4.4 Elastic constants for isotropic and transversely isotropic materials used in the analysis.....	26
Table 4.5 Normalized T-stress T_{11} and T_{33} of penny-shaped crack embedded in isotropic and transversely isotropic, linear elastic, infinite medium under uniform normal traction.....	26
Table 4.6 Normalized generalized T-stress T_{11} for spherical cap crack in linear piezoelectric infinite body under (i) uniform remote tension $\sigma_0 = 1 \times 10^6 \text{ N/m}^2$ and (ii) uniform remote tension $\sigma_0 = 1 \times 10^6 \text{ N/m}^2$ and uniform remote electric induction $d_0 = 1 \times 10^{-3} \text{ C/m}^2$	34
Table 4.7 Normalized generalized T-stress T_{33} for spherical cap crack in linear piezoelectric infinite body under (i) uniform remote tension $\sigma_0 = 1 \times 10^6 \text{ N/m}^2$ and (ii) uniform remote tension $\sigma_0 = 1 \times 10^6 \text{ N/m}^2$ and uniform remote electric induction $d_0 = 1 \times 10^{-3} \text{ C/m}^2$	35
Table 4.8 Normalized generalized T-stress T_{14} for spherical cap crack in linear piezoelectric infinite body under (i) uniform remote tension $\sigma_0 = 1 \times 10^6 \text{ N/m}^2$ and (ii) uniform remote tension $\sigma_0 = 1 \times 10^6 \text{ N/m}^2$ and uniform remote electric induction $d_0 = 1 \times 10^{-3} \text{ C/m}^2$	35

LIST OF FIGURE

Page

Figure 2.1 Schematic of isolated crack in piezoelectric infinite medium	11
Figure 2.2 Schematics indicating the decomposition of the original problem: (a) original problem, (b) <i>sub-problem1</i> , and (c) <i>sub-problem2</i>	12
Figure 3.1 Schematic of crack-tip element and local coordinate system for calculation of generalized T-stress.....	21
Figure 4.1 (a) Piezoelectric infinite body containing penny-shaped crack and (b) crack subjected to uniformly distributed pressure $t_3^+ = -t_3^- = \sigma_0$ and uniformly distributed surface electric charge $t_4^+ = -t_4^- = d_0$	24
Figure 4.2 Three meshes of penny-shaped crack used in numerical study; Mesh-1 containing 8 elements and 4 crack-tip elements, Mesh-2 containing 32 elements and 8 crack-tip elements, and Mesh-3 containing 128 elements and 16 crack-tip elements	24
Figure 4.3 (a) Schematic of infinite piezoelectric medium containing tunnel crack in $x_1 - x_2$ plane, (b) geometry of tunnel crack, and (c) tunnel crack subjected to uniform pressure $t_3^+ = -t_3^- = \sigma_0$ and uniform electric charge $t_4^+ = -t_4^- = d_0$	27
Figure 4.4 Three meshes of tunnel crack used in numerical study; Mesh-1 containing 32 elements with 16 crack-tip elements, Mesh-2 containing 128 elements with 32 crack-tip elements, and Mesh-3 containing 512 elements with 64 crack-tip elements	28
Figure 4.5 Normalized non-zero generalized T-stress of tunnel crack in PZT-4 under $\sigma_0 = 1 \times 10^6 \text{ N/m}^2$ and $d_0 = 0$	28
Figure 4.6 Normalized non-zero generalized T-stress of tunnel crack in PZT-5H under $\sigma_0 = 1 \times 10^6 \text{ N/m}^2$ and $d_0 = 0$	29
Figure 4.7 Normalized non-zero generalized T-stress of tunnel crack in PZT-4 under $\sigma_0 = 1 \times 10^6 \text{ N/m}^2$ and $d_0 = 1 \times 10^{-3} \text{ C/m}^2$	29
Figure 4.8 Normalized non-zero generalized T-stress of tunnel crack in PZT-5H under $\sigma_0 = 1 \times 10^6 \text{ N/m}^2$ and $d_0 = 1 \times 10^{-3} \text{ C/m}^2$	30
Figure 4.9 Normalized T_{11}/σ_0 of extended tunnel crack to plane strain problem in PZT-4 under $\sigma_0 = 1 \times 10^6 \text{ N/m}^2$	31
Figure 4.10 Normalized T_{11}/σ_0 of extended tunnel crack to plane strain problem in PZT-4 under $\sigma_0 = 1 \times 10^6 \text{ N/m}^2$	31

Figure 4.11 A linear piezoelectric, infinite body containing spherical cap crack.....	32
Figure 4.12 Spherical cap crack subjected to (a) uniform remote tension $\sigma_{33}^{\infty} = \sigma_0$, (b) uniform remote biaxial tension $\sigma_{11}^{\infty} = \sigma_{33}^{\infty} = \sigma_0$, and (c) uniform remote tension $\sigma_{33}^{\infty} = \sigma_0$ and uniform remote electric induction $\sigma_{34}^{\infty} = d_0$	33
Figure 4.13 Meshes of spherical cap crack used in analysis (schematics only show projected meshes on the $x_1 - x_2$ plane); Mesh-1 containing 16 elements with 8 crack-tip elements, Mesh-2 containing 32 elements with 8 crack-tip elements, and Mesh-3 containing 128 elements with 16 crack-tip elements.....	34
Figure 4.14 Normalized T_{11}/σ_0 , T_{33}/σ_0 and T_{13}/σ_0 for spherical cap crack subjected to uniform remote biaxial tension $\sigma_0 = 1 \times 10^6 \text{ N/m}^2$. Results are reported for PZT-4.	36
Figure 4.15 Normalized T_{14}/d_0 and T_{34}/d_0 for spherical cap crack subjected to uniform remote biaxial tension $\sigma_0 = 1 \times 10^6 \text{ N/m}^2$. Results are reported for PZT-4.	36
Figure 4.16 Normalized T_{11}/σ_0 , T_{33}/σ_0 and T_{13}/σ_0 for spherical cap crack subjected to uniform remote biaxial tension $\sigma_0 = 1 \times 10^6 \text{ N/m}^2$. Results are reported for PZT-5H.	37
Figure 4.17 Normalized T_{14}/d_0 and T_{34}/d_0 for spherical cap crack subjected to uniform remote biaxial tension $\sigma_0 = 1 \times 10^6 \text{ N/m}^2$. Results are reported for PZT-5H.	37
Figure 4.18 (a) A pair of identical co-planar circular cracks in transversely isotropic, linear piezoelectric, infinite domain and (b) body under uniform remote tension $\sigma_{33}^{\infty} = \sigma_0$	38
Figure 4.19 Three meshes of penny-shaped crack used in numerical study; Mesh-1 containing 16 elements with 8 crack-tip elements, Mesh-2 containing 64 elements with 16 crack-tip elements, and Mesh-3 containing 192 elements with 32 crack-tip elements.....	39
Figure 4.20 Normalized T_{11} for <i>Crack-B</i> in a pair of two identical co-planar circular cracks in linear piezoelectric infinite body under uniform remote tension $\sigma_0 = 1 \times 10^6 \text{ N/m}^2$. Results are reported for PZT-4 and PZT-5H.....	40
Figure 4.21 Normalized T_{33} for <i>Crack-B</i> in a pair of two identical co-planar circular cracks in linear piezoelectric infinite body under uniform remote tension $\sigma_0 = 1 \times 10^6 \text{ N/m}^2$. Results are reported for PZT-4 and PZT-5H.....	40

Figure 4.22 Normalized T_{13} for <i>Crack-B</i> in a pair of two identical co-planar circular cracks in linear piezoelectric infinite body under uniform remote tension $\sigma_0 = 1 \times 10^6 \text{ N/m}^2$. Results are reported for PZT-4.	41
Figure 4.23 Normalized T_{11} for <i>Crack-B</i> in a pair of two identical co-planar circular cracks in linear piezoelectric infinite body under uniform remote tension $\sigma_0 = 1 \times 10^6 \text{ N/m}^2$. Varies distance between cracks. Results are reported for PZT-4 and PZT-5H.	41
Figure 4.24 Normalized T_{33} for <i>Crack-B</i> in a pair of two identical co-planar circular cracks in linear piezoelectric infinite body under uniform remote tension $\sigma_0 = 1 \times 10^6 \text{ N/m}^2$. Varies distance between cracks. Results are reported for PZT-4 and PZT-5H.	42
Figure 4.25 Normalized T_{13} for <i>Crack-B</i> in a pair of two identical co-planar circular cracks in linear piezoelectric infinite body under uniform remote tension $\sigma_0 = 1 \times 10^6 \text{ N/m}^2$. Varies distance between cracks. Results are reported for PZT-4.	42
Figure 4.26 Normalized T_{13} for <i>Crack-B</i> in a pair of two identical co-planar circular cracks in linear piezoelectric infinite body under uniform remote tension $\sigma_0 = 1 \times 10^6 \text{ N/m}^2$. Varies distance between cracks. Results are reported for PZT-5H.	43

LIST OF ABBREVIATIONS

C_{mJ}^{tK}	kernel appearing in boundary integral equation
D_i	components of electric induction vector
E_i	components of electric field
E_{iJKm}	generalized moduli
E_{ijkm}	moduli of elastic material
e_{mij}	piezoelectric constants
G_{iK}^J	kernel appearing in boundary integral equation
H_{iK}^J	kernel appearing in boundary integral equation
n_i	components of unit normal vector
S_{iJ}^P	generalized stress Green's function
S_c^+, S_c^-	crack surfaces
t_J	components of generalized traction vector
t_j	components of traction vector
U_J^P	generalized displacement Green's function
u_j	components of displacement vector
u_K	components of generalized displacement
x	interior point of the body
z	unit vector normal to the position vector $\xi - x$
δ_{IJ}	standard Kronecker symbol
ε_{ij}	components of strain tensor
ε_{ijk}	standard alternating symbol
ϕ	electric potential
κ_{im}	dielectric permittivities
σ_{ij}	components of the stress tensor
ξ	point located on the crack surface

CHAPTER 1

INTRODUCTION

1.1 GENERAL

From the past three decades, highly advanced and multi-purposed materials have been continuously developed and also well-recognized in various fields including engineering and industrial applications. Piezoelectric materials are well-known examples of smart materials that have received significant popularity nowadays. Since the date of discovery of the piezoelectric effect by Jacques and Pierre Curie in 1880 and its inverse effect by Gabriel Lippmann in 1881, piezoelectric materials have been widely used as parts of many devices such as sensors (e.g., contact microphone, non-destructive testing devices, etc.), actuators (e.g., lever arm amplification, ultrasonic equipment, etc.), and the medical instruments such as hearing aid due to their outstanding properties and desirable electro-mechanical coupling effects. Besides those positive features, most of piezoelectric materials are found brittle in nature and generally possess low tensile strength and fracture toughness. This renders the high tendency of the development of damages/flaws within the materials during their applications and can finally cause the loss of integrity and reduction of their lifetime usage. Understanding of fracture mechanism/behavior of piezoelectric materials is, as a result, fundamental and can potentially be useful as an essential basis in the design procedure of piezoelectric components and devices.

Two commonly used approaches, based on either experimental investigations or mathematical modeling, have been widely applied to explore the basic fracture behavior of piezoelectric solids (e.g., Shindo *et al.*, 2007; Okayasu *et al.*, 2010; Lee *et al.*, 2011). While various techniques in the first group have proved to yield results reflecting real responses and behavior, cost associated with specimen preparation and experimental setup can be significant. Results obtained from experiments conducted at any scale are generally dependent on testing parameters and environments and the generalization of those results to describe different or practical scenarios can be limited. In addition, an experimental design to afford an extensive parametric study for the whole range of parameters of interest can lead to a large number of specimens required and it, finally, suffers from budget and time limitations. As a consequence, theoretical-based simulations via experimentally-

calibrated mathematical models have become attractive alternatives and been broadly used to examine the fracture phenomena in piezoelectric bodies.

The framework of piezoelectric fracture modeling has been well-established for several decades based on the hypothesis of linear piezoelectricity. In such linear theory, the stress and electric intensity factor are essential fracture data that not only completely describe the near-tip mechanical/electrical fields but also involve in the prediction of crack initiation and advances. Determination of both stress and electric intensity factors via either analytical or numerical techniques has been successfully established within the context of two- and three-dimensional crack models. Besides those intensity factors, the first non-singular term in such expansion, commonly known as the generalized T-stress, has recently gained significant attention from many researchers. It has been reviewed by various researchers that the T-stress term plays a vital role in the calculation of the plastic-zone size and shape, the stress tri-axiality ahead of the crack front, and the propagation direction of cracks in elastic media (e.g., Larsson and Carlsson, 1973; Cotterell and Rice, 1980). Ignorance of such parameter in the modeling can lead to inaccurate results or potentially mislead the response prediction. For cracks in piezoelectric media, the study by Zhu and Yang (1999) and Viola *et al.* (2008) also revealed the importance of the generalized T-stress in the prediction of crack kinking and the near-tip stress and electric induction field. These past evidences should indicate the necessity to integrate the generalized T-stresses in the mathematical models to enhance the response prediction of piezoelectric crack bodies.

Analogous to the determination of electric displacement and stress intensity factors, the generalized T-stress cannot be directly obtained from the asymptotic analysis of the near-tip field but it still requires solving a complete boundary value problem. Due to the complexity posed by the material anisotropy, singularity near the surface of discontinuities, and general body configurations and prescribed conditions, robust and efficient solution procedures are obligatory to perform the comprehensive analysis for associated fields and other related quantities. Boundary-integral-equation-based approaches are well-known computational procedures that have been proved efficient and robust for stress analysis of crack bodies. Their attractive feature results directly from that the key governing equation can be formulated only in terms of unknown functions on the domain boundary and surfaces of discontinuities. As a direct consequence, the reduction of one spatial dimension can be gained in the discretization procedure for constructing numerical solutions. In addition, these techniques allow the remote boundary and conditions

associated with an infinite body model to be treated in a simple manner; in particular, for an infinite body without the body source, the governing integral equation contains only unknown functions on the crack surface. These advantages render the boundary integral equation techniques popular and well recognized in the fracture analysis. The development of such techniques to have the capability to extract all essential fracture data along the crack front in an efficient and accurate manner is essential and should provide a powerful computational tool serving the investigation of cracks in piezoelectric media.

1.2 BACKGROUND AND REVIEW

This section mainly presents the summary of previous studies relevant to the current investigation in order to illustrate the historical development and the state of the art in the field of linear piezoelectric fracture analysis. The first part of this section focuses mainly on work towards the fracture analysis to determine the electric displacement and stress intensity factors whereas the last part presents previous studies focusing on the determination of the generalized T-stress. Although the present study does not directly involve the analysis for the intensity factors, results of the review in the first part should provide useful background, essential connection to the current study, and the breakthrough in this area.

1.2.1 Analysis for Intensity Factors in Piezoelectric Materials

In linear piezoelectric fracture mechanics, the electric displacement and stress intensity factors are essential parameters in the singular term of the asymptotic near-tip expansion that completely describes the dominant field along the crack boundary. Various approaches based on both analytical-based and numerical techniques have been proposed and successfully implemented to determine such fracture data for numerous scenarios. Xu and Rajapakse (1999) employed Lekhnitskii's complex potential representation to derive the analytical solution of an elliptical void in a two-dimensional, linear piezoelectric infinite medium under remote mechanical and electrical loading conditions. In their study, electrically impermeable, electrically permeable, and electrically semi-permeable conditions were considered and the special case of a crack can readily be obtained by taking proper limiting process of the void aspect ratio. Results from their study also indicated that under the pure mechanical loading condition, the stress intensity factor is independent of the electrical boundary conditions. Huang and Kuang (2003)

used an analytical continuation technique to investigate a straight mixed permeable-impermeable crack contained in a two-dimensional, transversely isotropic, linear, piezoelectric whole space. They pointed out that the singularity behavior appears at the junction of the impermeable and permeable boundaries. Chen *et al.* (2000) presented the complete solution of the mechanical/electrical field and non-zero intensity factors for a penny-shaped crack under uniform remote tension and electric displacement loading. They found, in their study, that material properties play no role on both electric displacement and stress intensity factors. Chen and Shioya (2000) reported the closed form solution of the electric and stress intensity factors for a circular crack in a three-dimensional, linear piezoelectric, unbounded domain subjected to arbitrary anti-symmetric loadings. Hou *et al.* (2001) used a reciprocal theorem to derive the exact solution of the intensity factors for a circular crack embedded in a transversely isotropic, linear piezoelectric whole space under the action of a concentrated force and a concentrated electric charge located and oriented arbitrarily on the crack surface. They also concluded that the non-zero stress intensity factor of a medium made of a piezoelectric material PZT4-E is higher than that of a body made of a pure elastic material PZT4. Later, Chen and Lim (2005) utilized the potential theory to derive the analytical solution of both electric displacement and stress intensity factors for a circular crack in a transversely isotropic, linear piezoelectric, infinite body subjected to a pair of normal concentrated loads on the crack face. These fundamental results were then applied to derive an explicit integral formula for a crack under arbitrarily distributed normal traction and the closed form solution for a crack under uniform pressure.

Due to the limited capability of analytical techniques to treat more practical situations, a variety of boundary element methods has been widely implemented to enhance the modeling versatility. A selected set of pertinent studies resulting from the extensive review is summarized here to indicate the breakthrough in the area (also see extensive review in Rungamornrat and Mear, 2008c; Phongtinnaboot *et al.*, 2011). For two-dimensional piezoelectric fracture modeling, following investigations have been well-recognized. Pan (1999) developed the single-domain, collocation-based, boundary element method to calculate both the electric and stress intensity factors of cracks in two-dimensional anisotropic finite bodies. In his study, all involved fundamental solutions were derived by a standard complex variable function approach. Later, Rajapakse and Xu (2001) derived the Green's function for both the line force and electric charge, and then applied such results to implement the boundary integral equation method to determine the energy release rate and

intensity factors for cracks in two-dimensional piezoelectric infinite media. The proposed technique was found to be capable of solving relatively complex crack problems (e.g., micro-crack clusters, forked cracks, and branched cracks). Davi and Milazzo (2001) developed the multi-domain-based boundary element technique using the generalized displacement boundary integral equation to solve cracks in two-dimensional piezoelectric finite bodies. The degeneracy of the conventional boundary integral equation technique when applied to piezoelectric crack problems was clearly demonstrated by Liu and Fan (2001) and the sub-domain technique was suggested to overcome such difficulty. Later, Groh and Kuna (2005) implemented a direct collocation boundary element scheme along with the domain decomposition strategy to solve cracks in bi-material piezo-composites and non-straight cracks. Quarter-point elements were utilized to enhance the accuracy of the approximation of the near-tip field.

For fully three-dimensional analysis of piezoelectric fracture problems, various schemes of boundary integral equation methods have been proposed. Techniques based on the use of generalized displacement integral equation along with the sub-domain strategy have been recognized (e.g., Sanz *et al.*, 2005; Wippler and Kuna, 2007); however, such methods can experience major difficulty when applied to solve multiple cracks and cracks with relatively complex geometry. In addition, partitioning the domain into several parts can significantly increase the number of extra unknowns along the partitioned surfaces and the treatment of the singularity of the unknown generalized traction ahead of the crack front requires special care. Single-domain boundary element methods have been increasingly developed to enhance the modeling capability and remedy the mathematical degeneracy posed by the conventional technique. Techniques based on hyper-singular integral formulations have been developed to solve cracks in both piezoelectric infinite and finite bodies (e.g., Chen, 2003a; Chen, 2003b; Qin and Noda, 2004; Zhao *et al.*, 2004; Qin *et al.*, 2007). While such computational procedures were implemented successfully, the numerical treatments are suffering from the strong requirements posed by the hyper-singular integrals (see discussion in Chen, 2003a and 2003b; Martin and Rizzo, 1996). Alternative boundary element methods based on singularity-reduced integral equations have also been proposed in the past two decades to solve cracks in three-dimensional piezoelectric media. This class of numerical procedures has received significant attention from various investigators due to their positive characteristics corresponding mainly to the reduction of smoothness requirements from the hyper-singular methods. Rungamornrat and Mear (2008c) implemented the first completely

regularized, symmetric Galerkin boundary element method (SGBEM) to analyze cracks in three-dimensional, generally anisotropic, linear piezoelectric domains. In their formulation, the key governing integral equation was systematically regularized to contain only weakly-singular kernels and this renders the use of continuous basis functions in the approximation of unknown functions on the crack surface. While their technique yielded highly accurate solutions of electric and stress intensity factors and was applicable to generally anisotropic materials, cracks of arbitrary geometry and general loading conditions, the formulation and implementation is principally limited to cracks in an infinite body. Later, Solis *et al.* (2009) presented a singularity-reduced boundary element approach to solve cracks in a finite body. In the regularization procedure, they employed the subtraction technique to remove the strong and hyper singularities. It worth noting that the validity of their final regularized integral equations still needs crack-face data of the type $C^{1-\alpha}$ and, additionally, their development is carried out only for transversely isotropic piezoelectric materials. Recently, Phongtinnaboot *et al.* (2011) generalized the work of Rungamornrat and Mear (2008c) to establish the weakly singular SGBEM for piezoelectric fracture analysis of finite bodies. Besides the capability to treat arbitrary shaped cracks and a general anisotropic constitutive material model, the key difference between their technique and that by Solis *et al.* (2009) is the smoothness requirement of the boundary data; in particular, C^0 -boundary data is only required for the validity of the integrals and in the solution approximation. Although the weakly-singular SGBEM has been well-developed for three-dimensional crack analysis and found robust and computationally efficient, the feature for calculating the generalized T-stress is still not available and, therefore, requires further development.

1.2.2 T-Stress in Piezoelectric Materials

In contrast to linear elastic fracture modeling, investigations related to the development of solution technique to determine the generalized T-stress is found relatively few. This should be due mainly to that the integration of such fracture data in the prediction of responses of cracked bodies is quite new and the complexity posed, in addition, by the anisotropic and fully coupled feature of the material constitutive law. Existing relevant studies resulting from an extensive literature survey can be summarized below. Zhu and Yang (1999) used the concept of the continuous dislocations and electric dipoles to develop a boundary integral equation scheme to examine the role of the generalized T-stress for a straight crack in a two-dimensional,

homogeneous, linear piezoelectric, whole space under remote mechanical and loading conditions. They pointed out that the generalized T-stress play a crucial role on the crack kinking angle. Later, Hao and Biao (2004) applied the superposition technique and Plemelj formulation to derive the analytical solution of the generalized T-stress for an impermeable straight crack contained in a transversely isotropic, linear piezoelectric whole space under remote mixed mechanical/electrical loading conditions. From their work, it was revealed that the value of the generalized T-stress is highly dependent on both elastic and electric material constants. Zhong and Li (2007) applied the Fourier integral transform along with the standard procedure for solving dual integral equations to obtain the closed form result of the generalized T-stress for a semi-permeable Griffith crack in two-dimensional, transversely isotropic, linear piezoelectric solids with magnetic effect. Both the remote uniform tension and electrical induction were investigated. They concluded, in this study, that the generalized T-stress in this coupling material is significantly different from that of the elastic material. Later, Viola *et al.* (2008) established an analytical technique via the transformation of similarity and representations in terms of analytic potentials to examine the effect of non-singular terms on the mechanical and electrical fields of the Griffith crack in two-dimensional, transversely isotropic, piezoelectric infinite media under remote biaxial loading. They revealed that such non-singular part, induced by the biaxial loading, has the strong influence on the hoop stress, the elastic and electric displacements, and stress component collinear to the crack. In addition, they concluded that ignorance of the non-singular terms can mislead the prediction of the direction of crack advances since the influence of bi-axiality resulting from the prescribed load is fully neglected. Recently, Liu *et al.* (2012) employed the complex variable function approach to construct the complete solution of mechanical/electrical fields of an elliptical void and a crack under uniform pressure. Results from their extensive investigation confirmed that the non-singular term can play a vital role on the behavior of the near-tip stress and electric induction.

From a careful literature search, studies regarding to the development of analytical and numerical techniques for calculating the generalized T-stress for the three-dimensional case has not been recognized. Lack of such solution methodology clearly limits the in-depth investigation of the influence of the generalized T-stress within the context of fully three-dimensional models; in particular, various three-dimensional aspects such as the non-planarity of the crack surface, stress tri-axiality ahead of the crack front, and full mode-mixity cannot be explored. This existing gap

of knowledge, concerning mainly to the development of general, promising solution procedures, encourages the present study.

1.3 OBJECTIVES

The key objective of the current investigation is to establish an accurate and efficient computational technique capable of computing the generalized T-stress of cracks in piezoelectric media

1.4 SCOPE OF RESEARCH

The proposed investigation is limited only to (i) a three-dimensional, homogeneous, infinite medium, (ii) impermeable cracks, (iii) a body without the body force and body electric charge, and (iv) piezoelectric materials governed by linear constitutive law.

1.5 METHODOLOGY AND PROCEDURE

Fundamental theories, basic assumptions, key methodology and research procedures essential for the current study are indicated below.

- 1) Basic field equations are obtained from theory of linear piezoelectricity;
- 2) Singularity-reduced integral relations/equations for discontinuities in an anisotropic, linear piezoelectric, infinite domain without the remote loading is developed using the regularization procedure proposed by Rungamornrat and Mear (2008c) ;
- 3) The influence of the remote loading conditions is treated by using the superposition technique;
- 4) A system of integral equations governing both the unknown jump and sum of generalized displacements on both surfaces of the crack is formulated using the results from 2);
- 5) A well-known weakly singular SGBEM is implemented first to solve the governing integral equation for the jump of the generalized traction to obtain the unknown relative crack-face the generalized displacement. The accuracy of the approximation of the near-tip relative crack-face generalized displacement is enhanced by using special shape functions developed by Rungamornrat and Mear (2008c) ;
- 6) The weak-form generalized displacement integral equation is solved along with the known information of the relative crack-face displacement using standard Galerkin procedure;

- 7) Explicit formula for extracting the generalized T-stress is established in terms of the gradient of sum of the generalized displacement along the crack front;
- 8) An in-house computer code is implemented to verify the formulation and the weakly singular SGBEM; and
- 9) Extensive numerical experiments are conducted to verify the implemented numerical procedure and investigate its computational performance.

1.6 RESEARCH SIGNIFICANCE

The main contribution of the current study is to offer an accurate and efficient computational tool capable of calculating the generalized T-stress of arbitrary shaped cracks in three-dimensional infinite bodies made of fully anisotropic piezoelectric materials. The computational tool of this high capability should be potentially useful for the modeling of crack propagation supplemented by sophisticated growth laws involving the nonsingular term. In addition, this research should provide the fundamental basis for the further development of advanced numerical techniques applicable to treat more complex and large scale fracture problems, e.g. cracks in finite bodies.

CHAPTER 2

PROBLEM FORMULATION

This chapter summarizes the clear description of the boundary value problem, basic field equations governing the behavior of linear piezoelectric media, crack-face boundary conditions, the standard integral relations for generalized displacements and generalized stresses, the regularization of related integral relations/equations, and the formulation of the key governing for piezoelectric cracked body.

2.1 BASIC EQUATIONS FOR LINEAR PIEZOELECTRICITY

Basic field equations governing all involved field quantities are taken from the theory of linear piezoelectricity. For a medium subjected to zero body forces and body electric charges, those equations take the following forms

$$\sigma_{ij,i} = 0; \quad D_{i,i} = 0 \quad (2.1)$$

$$\sigma_{ij} = E_{ijkl} \varepsilon_{kl} - e_{mij} E_m; \quad D_i = e_{ikm} \varepsilon_{km} + \kappa_{im} E_m \quad (2.2)$$

$$\varepsilon_{ij} = \frac{1}{2}(u_{i,j} + u_{j,i}); \quad E_i = -\phi_{,i} \quad (2.3)$$

where σ_{ij} , ε_{ij} , and u_i are components of the stress tensor, the strain tensor, and the displacement vector, respectively; D_i , E_i and ϕ represent components of the electric induction vector, components of the electric field and the electric potential, respectively; E_{ijkl} , e_{mij} , and κ_{im} denote the elastic moduli, piezoelectric constants, and dielectric permittivities of the constituting material, respectively; and the comma notation $(\cdot)_{,i}$ represents partial derivatives with respect to the reference Cartesian coordinate x_i and the standard rules of indicial notations apply throughout (i.e., any lower case index takes the values 1, 2, 3, and repeated indices imply the summation over their range). By following the notations introduced by Rungamornrat and Mear (2008c), the above field equations can be expressed in the following concise form

$$\sigma_{iJ,i} = 0 \quad (2.4)$$

$$\sigma_{iJ} = E_{iJKm} u_{K,m} \quad (2.5)$$

where any upper case index takes the value 1, 2, 3, 4 and the summation over their range is implied for any repeated index; σ_{iJ} is termed the generalized stress that

combines the stress σ_{ij} and the electric induction $\sigma_{i4} \equiv D_i$; u_j is termed the generalized displacement that combines the displacement u_j and the electric potential $u_4 \equiv \phi$; and E_{ijkl} is termed the generalized moduli that combines the elastic moduli E_{ijkl} , the piezoelectric constants $E_{ij4l} \equiv e_{ijl}$ and the dielectric permittivities $E_{i44l} \equiv -\kappa_{il}$. It is remarked that the constitutive relation in terms of the generalized displacement gradient (2.5) can be derived by substituting (2.3) into (2.2). To be consistent with this concise notation, the generalized surface traction t_j on the smooth surface with the outward unit normal vector \mathbf{n} is defined by $t_j = \sigma_{ij} n_i$. Clearly, the generalized traction t_j consists of the traction $t_j = \sigma_{ij} n_i$ and the surface electric charge $t_4 \equiv \sigma_{i4} n_i = D_i n_i$.

2.2 PROBLEM DESCRIPTION

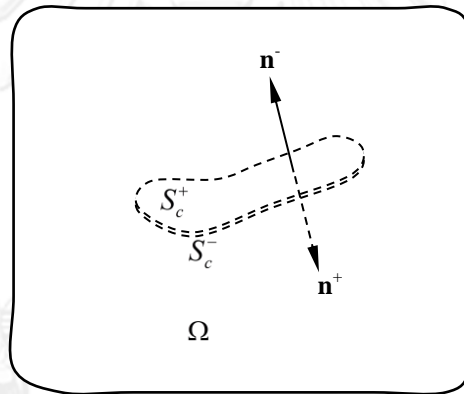


Figure 2.1 Schematic of isolated crack in piezoelectric infinite medium

Consider a three-dimensional, infinite body Ω containing a crack as depicted in Figure 2.1. The domain is made of a homogeneous, generally anisotropic, linear piezoelectric solid with known material constants. The embedded crack is represented mathematically by two coincident, sufficiently smooth surfaces S_c^+ and S_c^- with the (outward) unit normal vector denoted by \mathbf{n}^+ and \mathbf{n}^- , respectively. The body is subjected to zero body force and body electric charge fields but subjected to the prescribed remote generalized stress σ_{ij}^∞ . In addition, the impermeable crack-face condition is considered (i.e., the generalized tractions on both crack surfaces S_c^+ and S_c^- , denoted respectively by t_j^+ and t_j^- , are fully prescribed). It should be remarked that while only a single crack is shown schematically in Figure 2.1, the

development to follow can essentially treat multiple cracks by simply considering S_c^+ and S_c^- as the union of all crack surfaces.

2.3 TREATMENT OF REMOTE CONDITION

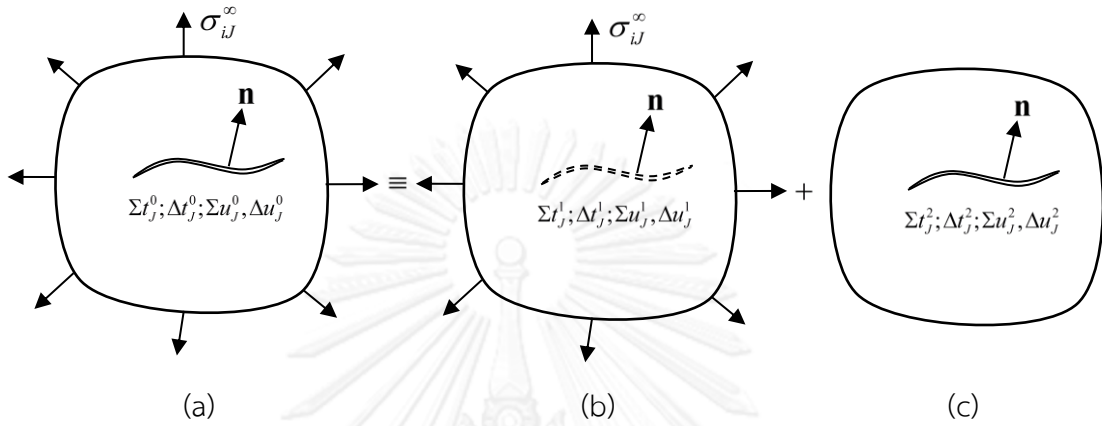


Figure 2.2 Schematics indicating the decomposition of the original problem:

(a) original problem, (b) *sub-problem1*, and (c) *sub-problem2*

Due to the linearity of the basic field equations, the original problem can be separated into two different problems, denoted by *sub-problem1* and *sub-problem2* as shown in Figure 2.2. The *sub-problem1* is associated with the uncracked infinite body subjected only to the remote generalized stress σ_{ij}^∞ whereas the *sub-problem2* corresponds to an infinite body containing the same crack as the original problem but subjected only to the proper generalized tractions t_j^{+2} and t_j^{-2} on the surfaces S_c^+ and S_c^- , respectively. From the method of superposition, the crack-face data for all three problems can be related by

$$\Sigma t_j^0 = \Sigma t_j^1 + \Sigma t_j^2 \quad (2.6)$$

$$\Delta t_j^0 = \Delta t_j^1 + \Delta t_j^2 \quad (2.7)$$

$$\Sigma u_j^0 = \Sigma u_j^1 + \Sigma u_j^2 \quad (2.8)$$

$$\Delta u_j^0 = \Delta u_j^1 + \Delta u_j^2 \quad (2.9)$$

where the symbols “ Δ ” and “ Σ ” are used to emphasize the jump and sum of crack-face quantities and the superscript “0”, “1” and “2” are employed to indicate the quantities associated with the original problem, the *sub-problem1* and the *sub-problem2*, respectively. It is worth noting that the complete mechanical/electrical field of the *sub-problem1* can be trivially obtained in a closed form; in particular,

$\Sigma t_j^1 = 0$, $\Delta t_j^1 = 2\sigma_{ij}^\infty n_i$ and $\Delta u_j^2 = 0$. However, to obtain the complete solution of the original problem, it still remains to solve the non-trivial *sub-problem2*. The formulation and implementation of the numerical technique developed further below is, therefore, restricted mainly to the *sub-problem2* in which the remote mechanical/electrical loading vanishes and the superscript “2” is dropped for simplicity. Note in addition that from the relations (2.6) and (2.7), the prescribed Σt_j^0 and Δt_j^0 resulting from the impermeable crack-face condition, and the solved Σt_j^1 and Δt_j^1 , the sum and jump of the generalized traction Σt_j^2 and Δt_j^2 are obviously prescribed whereas the sum and jump of the generalized displacement Σu_j^2 and Δu_j^2 are unknown a priori.

2.4 STANDARD INTEGRAL RELATIONS

By generalizing the Somigliana’s identity to the linear piezoelectricity, the generalized displacement at a point \mathbf{x} within an infinite cracked body that is subjected to zero generalized body force field (i.e., zero body force and zero body electric charge) and remote loading is given by

$$u_p(\mathbf{x}) = \int_{S_c^+} U_j^P(\xi - \mathbf{x}) \Sigma t_j(\xi) dA(\xi) - \int_{S_c^+} S_{ij}^P(\xi - \mathbf{x}) n_i(\xi) \Delta u_j(\xi) dA(\xi) \quad (2.10)$$

where $U_j^P(\xi - \mathbf{x})$ and $S_{ij}^P(\xi - \mathbf{x})$ are known fundamental solutions (or Green’s functions) of the generalized displacements and stresses. The explicit expressions of $U_j^P(\xi - \mathbf{x})$ and $S_{ij}^P(\xi - \mathbf{x})$, for general anisotropic piezoelectric materials, are given by (see also the work of Deeg, 1980)

$$U_j^P(\xi - \mathbf{x}) = \frac{1}{8\pi^2 r} \oint_{z \cdot r=0} (\mathbf{z}, \mathbf{z})_{JP}^{-1} ds(\mathbf{z}) \quad (2.11)$$

$$S_{ij}^P(\xi - \mathbf{x}) = E_{ijkl} \frac{\partial U_k^P(\xi - \mathbf{x})}{\partial \xi_l} \quad (2.12)$$

where $\mathbf{r} = \xi - \mathbf{x}$, $r = |\mathbf{r}|$, \mathbf{z} is a unit vector on the plane normal to the position vector \mathbf{r} , $(\mathbf{z}, \mathbf{z})_{JP} = z_i E_{iJP} z_l$, and $(\mathbf{z}, \mathbf{z})^{-1}$ denotes an inverse of the matrix (\mathbf{z}, \mathbf{z}) . It should be remarked that the Green’s functions $U_j^P(\xi - \mathbf{x})$ and $S_{ij}^P(\xi - \mathbf{x})$ are singular at a point $\xi = \mathbf{x}$ of order $\mathcal{O}(1/r)$ and $\mathcal{O}(1/r^2)$, respectively. The boundary integral relation (2.10) allows generalized displacements at an interior point of the domain to be obtained once the unknown relative crack-face generalized displacement is

known. By taking a proper limit process $\mathbf{x} \rightarrow \mathbf{y} \in S_c^+$, it yields the boundary integral equation for the sum of the generalized displacement $\Sigma \mathbf{u}_p$:

$$\frac{1}{2} \Sigma \mathbf{u}_p(\mathbf{y}) = \int_{S_c^+} U_J^P(\boldsymbol{\xi} - \mathbf{y}) \Sigma t_J(\boldsymbol{\xi}) dA(\boldsymbol{\xi}) - \int_{S_c^+} S_{ij}^P(\boldsymbol{\xi} - \mathbf{y}) n_i(\boldsymbol{\xi}) \Delta u_J(\boldsymbol{\xi}) dA(\boldsymbol{\xi}) \quad (2.13)$$

The integral equation (2.13) possesses following features: (i) it involves only the known sum of the generalized traction Σt_p ; (ii) it contains two unknown functions $\Sigma \mathbf{u}_p$ and $\Delta \mathbf{u}_p$; (iii) the first integral involves the weakly singular kernel $U_J^P(\boldsymbol{\xi} - \mathbf{y})$ and can be interpreted in the sense of Riemann; and (iv) the second integral involves the strongly singular kernel $S_{ij}^P(\boldsymbol{\xi} - \mathbf{y})$ and must be interpreted in the sense of Cauchy. It is evident that only the integral relation (2.13) cannot be sufficiently employed to solve both unknowns $\Sigma \mathbf{u}_p$ and $\Delta \mathbf{u}_p$ on the crack surface. It is also worth remarking that the integral relation (2.13) cannot differentiate two problems involving the same crack subjected to different self-equilibrated, generalized tractions (i.e., $\Sigma t_J = \mathbf{0}$ for both cases).

To overcome such difficulty, an additional boundary integral equation must be established. By substituting the integral relation (2.10) into the constitutive law (2.5) and then invoking properties of both Green's functions $U_J^P(\boldsymbol{\xi} - \mathbf{x})$ and $S_{ij}^P(\boldsymbol{\xi} - \mathbf{x})$, it leads to the generalized stress integral relation at any point \mathbf{x} within the domain:

$$\sigma_{IK}(\mathbf{x}) = - \int_{S_c^+} S_{ij}^K(\boldsymbol{\xi} - \mathbf{x}) \Sigma t_J(\boldsymbol{\xi}) dA(\boldsymbol{\xi}) + \int_{S_c^+} \Sigma_{ij}^{IK}(\boldsymbol{\xi} - \mathbf{x}) n_i(\boldsymbol{\xi}) \Delta u_J(\boldsymbol{\xi}) dA(\boldsymbol{\xi}) \quad (2.14)$$

where the two-point function $\Sigma_{ij}^{IK}(\boldsymbol{\xi} - \mathbf{x})$ is given by

$$\Sigma_{ij}^{IK}(\boldsymbol{\xi} - \mathbf{x}) = E_{IKPq} \frac{\partial S_{ij}^P(\boldsymbol{\xi} - \mathbf{x})}{\partial \xi_q} \quad (2.15)$$

It results directly from the singularity behavior of $S_{ij}^P(\boldsymbol{\xi} - \mathbf{x})$ that the two-point function $\Sigma_{ij}^{IK}(\boldsymbol{\xi} - \mathbf{x})$ is singular at a point $\boldsymbol{\xi} = \mathbf{x}$ of order $\mathcal{O}(1/r^3)$. The integral relation (2.14) can be used to post-process for the generalized stress at any point within the body once the unknown $\Delta \mathbf{u}_J$ is solved. By multiplying equation (2.14) with a unit normal vector \mathbf{n}^+ at any point $\mathbf{y} \in S_c^+$ and then evaluating the limit $\mathbf{x} \rightarrow \mathbf{y} \in S_c^+$, it yields the integral equation of the jump in the generalized traction across the crack surface Δt_K :

$$\frac{1}{2} \Delta t_K(\mathbf{y}) = - \int_{S_c^+} S_{ij}^K(\boldsymbol{\xi} - \mathbf{y}) n_i(\mathbf{y}) \Sigma t_j(\boldsymbol{\xi}) dA(\boldsymbol{\xi}) + \int_{S_c^+} \Sigma_{ij}^{IK}(\boldsymbol{\xi} - \mathbf{y}) n_i(\mathbf{y}) n_j(\boldsymbol{\xi}) \Delta u_j(\boldsymbol{\xi}) dA(\boldsymbol{\xi}) \quad (2.16)$$

The boundary integral equation (2.16) possesses following features: (i) it contain the complete information of the generalized traction Δt_K and Σt_j ; (ii) it contains only one unknown function Δu_j ; (iii) the first integral involves the strongly singular kernel $S_{ij}^P(\boldsymbol{\xi} - \mathbf{y})$ and must be interpreted in the sense of Cauchy; and (iv) the second integral involves the hyper-singular kernel $\Sigma_{ij}^{IK}(\boldsymbol{\xi} - \mathbf{y})$ and must be interpreted in the sense of Hadamard finite part. It is evident that the integral equation (2.16) can be used to determine the jump in the generalized displacement Δu_j and, when applied along with (2.13), the sum of the generalized displacement Σu_p can also be obtained. It is crucial to remark that use of the standard boundary integral equations (2.13) and (2.16) in the formulation, it is unavoidable to treat both strongly singular and hyper-singular integrals in the numerical implementations.

2.5 REGULARIZED INTEGRAL RELATIONS/EQUATIONS

To suit the development of weakly singular SGBEM, a set of singularity-reduced, boundary integral equations must be established. A systematic regularization procedure for the case of linear piezoelectricity was proposed by Rungamornrat and Mear (2008c) and Phongtinnaboot *et al.* (2011) in their study of cracks in piezoelectric infinite and finite bodies. Such strategy is utilized in the present investigation and certain key components are briefly presented here.

In the regularization procedure, the strongly singular kernel $S_{ij}^P(\boldsymbol{\xi} - \mathbf{x})$ and the hyper-singular kernel $\Sigma_{ij}^{IK}(\boldsymbol{\xi} - \mathbf{x})$ are represented in following form:

$$S_{ij}^P(\boldsymbol{\xi} - \mathbf{x}) = H_{ij}^P(\boldsymbol{\xi} - \mathbf{x}) + \varepsilon_{ism} \frac{\partial G_{mj}^P(\boldsymbol{\xi} - \mathbf{x})}{\partial \xi_s} \quad (2.17)$$

$$\Sigma_{ij}^{IK}(\boldsymbol{\xi} - \mathbf{x}) = -E_{ijkl} \delta(\boldsymbol{\xi} - \mathbf{x}) + \varepsilon_{ism} \frac{\partial}{\partial \xi_s} \varepsilon_{lrs} \frac{\partial}{\partial \xi_r} C_{mj}^{IK}(\boldsymbol{\xi} - \mathbf{x}) \quad (2.18)$$

where $\delta(\boldsymbol{\xi} - \mathbf{x})$ is a three-dimensional Dirac-delta function with the center at a point \mathbf{x} , ε_{ism} is an alternating tensor; and functions $H_{ij}^P(\boldsymbol{\xi} - \mathbf{x})$, $G_{mj}^P(\boldsymbol{\xi} - \mathbf{x})$ and $C_{mj}^{IK}(\boldsymbol{\xi} - \mathbf{x})$ are given by

$$H_{ij}^P(\boldsymbol{\xi} - \mathbf{x}) = -\frac{1}{4\pi r^3} \delta_{jp} (\xi_i - x_i) \quad (2.19)$$

$$G_{mJ}^P(\xi - \mathbf{x}) = \frac{\varepsilon_{mqd} E_{qJKl}}{8\pi^2 r} \oint_{z:r=0} (\mathbf{z}, \mathbf{z})_{KP}^{-1} z_a z_l ds(\mathbf{z}) \quad (2.20)$$

$$C_{mJ}^{tK}(\xi - \mathbf{x}) = \frac{A_{mstl}^{KJPQ}}{8\pi^2 r} \oint_{z:r=0} (\mathbf{z}, \mathbf{z})_{PQ}^{-1} z_s z_l ds(\mathbf{z}) \quad (2.21)$$

in which A_{mstl}^{KJPQ} is a moduli-dependent constant defined by

$$A_{mstl}^{KJPQ} = \varepsilon_{aum} \varepsilon_{adt} \left\{ E_{uKPs} E_{dJQl} - \frac{1}{4} E_{dJKu} E_{lPQs} \right\} \quad (2.22)$$

Clearly, the function $H_{ij}^P(\xi - \mathbf{x})$ is independent of material properties and singular at point $\xi = \mathbf{x}$ of order $\mathcal{O}(1/r^2)$ whereas $G_{mJ}^P(\xi - \mathbf{x})$ and $C_{mJ}^{tK}(\xi - \mathbf{x})$ are singular at point $\xi = \mathbf{x}$ of order $\mathcal{O}(1/r)$. The existence of the representations (2.17) and (2.18) and the means for determining the functions $G_{mJ}^P(\xi - \mathbf{x})$ and $C_{mJ}^{tK}(\xi - \mathbf{x})$ for general anisotropy can be found in the investigations of Rungamornrat and Mear (2008a) and Rungamornrat and Senjuntichai (2009).

To construct the singularity-reduced, boundary integral relations for both generalized displacements and generalized stresses, the representations (2.17) and (2.18) are employed to aid the integration by parts procedure of the conventional integral relations (2.10) and (2.14) via Stokes' theorem to shift the derivatives from the functions $G_{mJ}^P(\xi - \mathbf{x})$ and $C_{mJ}^{tK}(\xi - \mathbf{x})$ to the crack-face data (see details of the development in Rungamornrat and Mear, 2008a). The final results are given by

$$u_p(\mathbf{x}) = \int_{S_c^+} U_J^P(\xi - \mathbf{x}) \Sigma t_J(\xi) dA(\xi) - \int_{S_c^+} H_{ij}^P(\xi - \mathbf{x}) n_i(\xi) \Delta u_J(\xi) dA(\xi) + \int_{S_c^+} G_{mJ}^P(\xi - \mathbf{x}) D_m \Delta u_J(\xi) dA(\xi) \quad (2.23)$$

$$\sigma_{iK}(\mathbf{x}) = \varepsilon_{irt} \frac{\partial}{\partial x_r} \left\{ \int_{S_c^+} G_{iK}^J(\xi - \mathbf{x}) \Sigma t_J(\xi) dA(\xi) + \int_{S_c^+} C_{mJ}^{tK}(\xi - \mathbf{x}) D_m \Delta u_J(\xi) dA(\xi) \right\} - \int_{S_c^+} H_{iK}^J(\xi - \mathbf{x}) \Sigma t_J(\xi) dA(\xi) \quad (2.24)$$

This set of singularity-reduced boundary integral relations offers an alternative to the standard integral relations (2.10) and (2.14) for post-processing the generalized displacements and stresses at any point within the medium once the unknown Δu_J is determined.

An alternative form of the integral equation for the sum of the generalized displacement (2.13) is obtained by first evaluating the proper limit $\mathbf{x} \rightarrow \mathbf{y} \in S_c^+$ of the integral relation (2.23), then multiplying the equation by a well-behaved test function \tilde{t}_p , and finally integrating the results over the upper surface of the crack. The final weakly singular weak-form boundary integral equation takes the following form

$$\begin{aligned} \frac{1}{2} \int_{S_c^+} \tilde{t}_p(\mathbf{y}) \Sigma u_p(\mathbf{y}) dA(\mathbf{y}) &= \int_{S_c^+} t_p(\mathbf{y}) \int_{S_c^+} U_J^P(\boldsymbol{\xi} - \mathbf{y}) \Sigma t_J(\boldsymbol{\xi}) dA(\boldsymbol{\xi}) dA(\mathbf{y}) \\ &\quad - \int_{S_c^+} t_p(\mathbf{y}) \int_{S_c^+} H_{ij}^P(\boldsymbol{\xi} - \mathbf{y}) n_i(\boldsymbol{\xi}) \Delta u_J(\boldsymbol{\xi}) dA(\boldsymbol{\xi}) dA(\mathbf{y}) \\ &\quad + \int_{S_c^+} t_p(\mathbf{y}) \int_{S_c^+} G_{mj}^P(\boldsymbol{\xi} - \mathbf{y}) D_m \Delta u_J(\boldsymbol{\xi}) dA(\boldsymbol{\xi}) dA(\mathbf{y}) \end{aligned} \quad (2.25)$$

Similarly, the alternative form of the integral equation for the jump of the generalized traction (2.16) is established by first evaluating the proper limit $\mathbf{x} \rightarrow \mathbf{y} \in S_c^+$ of the quantity $\sigma_{iK}(\mathbf{x}) n_i^+(\mathbf{y})$ via the integral relation (2.24), then multiplying the equation by an arbitrary well-behaved test function \tilde{u}_K , and finally integrating the results over the surface of the crack and then applying Stokes' theorem to carry out the integration by parts. The final result is given by

$$\begin{aligned} \frac{1}{2} \int_{S_c^+} \tilde{u}_K(\mathbf{y}) \Delta t_K(\mathbf{y}) dA(\mathbf{y}) &= - \int_{S^+} D_i \tilde{v}_K(\mathbf{y}) \int_{S^+} C_{mJ}^{iK}(\boldsymbol{\xi} - \mathbf{y}) D_m \Delta u_J(\boldsymbol{\xi}) dA(\boldsymbol{\xi}) dA(\mathbf{y}) \\ &\quad - \int_{S^+} D_i \tilde{v}_K(\mathbf{y}) \int_{S^+} G_{iK}^J(\boldsymbol{\xi} - \mathbf{y}) \Sigma t_J(\boldsymbol{\xi}) dA(\boldsymbol{\xi}) dA(\mathbf{y}) \\ &\quad - \int_{S^+} \tilde{v}_K(\mathbf{y}) \int_{S^+} H_{iK}^J(\boldsymbol{\xi} - \mathbf{y}) n_i(\mathbf{y}) \Sigma t_J(\boldsymbol{\xi}) dA(\boldsymbol{\xi}) dA(\mathbf{y}) \end{aligned} \quad (2.26)$$

It is vital to note that the weak-form boundary integral equations (2.25) and (2.26) are fully regularized in that all appearing kernels, $U_J^P(\boldsymbol{\xi} - \mathbf{y})$, $H_{ij}^P(\boldsymbol{\xi} - \mathbf{y}) n_i(\boldsymbol{\xi})$, $H_{iK}^J(\boldsymbol{\xi} - \mathbf{y}) n_i(\mathbf{y})$, $G_{mj}^P(\boldsymbol{\xi} - \mathbf{y})$ and $C_{mJ}^{iK}(\boldsymbol{\xi} - \mathbf{y})$, are only weakly singular of order $\mathcal{O}(1/r)$. This pair of weak-form integral equations provides a complete basis for the formulation of boundary value problems of cracks in piezoelectric infinite media.

CHAPTER 3

DEVELOPMENT OF WEAKLY SINGULAR SGBEM

This chapter devotes mainly to the solution methodology, the development of a numerical procedure based on the well-known weakly singular symmetric Galerkin boundary element method (SGBEM), and the post-process for the generalized T-stress. Essential components including the discretization, numerical integration and evaluation of all involved kernels are also discussed.

3.1 SOLUTION METHODOLOGY

A pair of weak-form integral equations, one for the sum of the crack-face generalized displacement (2.25) and the other for the relative crack-face generalized traction (2.26), provides a complete set of governing equations for determining the crack-face data Σu_p and Δu_p . For convenience in further reference, (2.25) and (2.26) are re-expressed in a more concise form as

$$\mathcal{D}(\tilde{t}, \Sigma u) = \mathcal{U}(\tilde{t}, \Sigma t) + \mathcal{G}(\tilde{t}, \Delta u) + \mathcal{H}(\tilde{t}, \Delta u) \quad (3.1)$$

$$\mathcal{C}(\tilde{u}, \Delta u) = \mathcal{G}(\Sigma t, \tilde{u}) + \mathcal{H}(\Sigma t, \tilde{u}) + \mathcal{D}(\tilde{u}, \Delta t) \quad (3.2)$$

where all involved linear and bilinear integral operators are defined by

$$\mathcal{U}(\mathbf{X}, \mathbf{Y}) = \int_{S_c^+} X_p(\mathbf{y}) \int_{S_c^+} U_J^p(\boldsymbol{\xi} - \mathbf{y}) Y_J(\boldsymbol{\xi}) dA(\boldsymbol{\xi}) dA(\mathbf{y}) \quad (3.3)$$

$$\mathcal{C}(\mathbf{X}, \mathbf{Y}) = - \int_{S^+} D_r X_K(\mathbf{y}) \int_{S^+} C_{mj}^{rk}(\boldsymbol{\xi} - \mathbf{y}) D_m Y_J(\boldsymbol{\xi}) dA(\boldsymbol{\xi}) dA(\mathbf{y}) \quad (3.4)$$

$$\mathcal{G}(\mathbf{X}, \mathbf{Y}) = \int_{S_c^+} X_p(\mathbf{y}) \int_{S_c^+} G_{mj}^p(\boldsymbol{\xi} - \mathbf{y}) D_m Y_J(\boldsymbol{\xi}) dA(\boldsymbol{\xi}) dA(\mathbf{y}) \quad (3.5)$$

$$\mathcal{H}(\mathbf{X}, \mathbf{Y}) = - \int_{S_c^+} X_p(\mathbf{y}) \int_{S_c^+} H_{ij}^p(\boldsymbol{\xi} - \mathbf{y}) n_i(\boldsymbol{\xi}) Y_J(\boldsymbol{\xi}) dA(\boldsymbol{\xi}) dA(\mathbf{y}) \quad (3.6)$$

$$\mathcal{D}(\mathbf{X}, \mathbf{Y}) = \frac{1}{2} \int_{S_c^+} X_K(\mathbf{y}) Y_K(\mathbf{y}) dA(\mathbf{y}) \quad (3.7)$$

where \mathbf{X} and \mathbf{Y} are any vectors. It is evident from (3.4) and (3.7) that the integral operators \mathcal{C} and \mathcal{D} are in a symmetric form, i.e., $\mathcal{C}(\mathbf{X}, \mathbf{Y}) = \mathcal{C}(\mathbf{Y}, \mathbf{X})$ and $\mathcal{D}(\mathbf{X}, \mathbf{Y}) = \mathcal{D}(\mathbf{Y}, \mathbf{X})$. While the system of equations (3.1) and (3.2) is coupled through the relative crack-face generalized displacement Δu_p , the generalized traction integral

equation (3.2) does not contain the sum of the generalized displacement $\Sigma \mathbf{u}_p$. As a result, the jump $\Delta \mathbf{u}_p$ is obtained first by solving (3.2) numerically using standard weakly singular SGBEM (see also Rungamornrat and Mear, 2008a and 2008b). After $\Delta \mathbf{u}_p$ is determined, the sum of the generalized displacement $\Sigma \mathbf{u}_p$ is obtained by solving (3.1) numerically using standard Galerkin procedure. Once the crack-face data is known, the generalized T-stress can be post-processed from $\Sigma \mathbf{u}_p$ in the neighborhood of the crack front.

3.2 DISCRETIZATION

By following standard Galerkin approximation procedure, a pair of boundary integral equations (3.1) and (3.2) can be discretized into the following systems of linear algebraic equations:

$$[\mathbf{D}][\Sigma \mathbf{U}] = [\mathbf{U} \quad \mathbf{G} + \mathbf{H}] \begin{bmatrix} \Sigma \mathbf{T} \\ \Delta \mathbf{U} \end{bmatrix} \quad (3.8)$$

$$[\mathbf{C}][\Delta \mathbf{U}] = [\mathbf{G} + \mathbf{H} \quad \mathbf{D}^*] \begin{bmatrix} \Sigma \mathbf{T} \\ \Delta \mathbf{T} \end{bmatrix} \quad (3.9)$$

where $\mathbf{C}, \{\mathbf{D}, \mathbf{D}^*\}, \mathbf{G}, \mathbf{H}, \mathbf{U}$ are known coefficient matrices obtained from linear integral operators $\mathcal{C}, \mathcal{D}, \mathcal{G}, \mathcal{H}, \mathcal{U}$, respectively; $\Delta \mathbf{U}$ and $\Sigma \mathbf{U}$ are unknown vectors of nodal quantities of the jump and sum of crack-face generalized displacements, respectively; and $\Delta \mathbf{T}$ and $\Sigma \mathbf{T}$ are known vectors of nodal quantities corresponding to the jump and sum of the crack-face generalized traction, respectively. Due to the weak singularity of (3.1) and (3.2), all crack-face data including the test functions are approximated by continuous, element-based, basis functions following standard finite element procedure (e.g., Oden and Carey, 1984; Hughes, 2000; Zienkiewicz and Taylor, 2000). In particular, standard isoparametric elements are exploited to approximate the crack-face data $\{\Sigma \mathbf{t}_j, \Delta \mathbf{t}_j, \Sigma \mathbf{u}_j, \Delta \mathbf{u}_j\}$ and the test functions $\{\tilde{\mathbf{u}}_k, \tilde{\mathbf{t}}_k\}$ for the majority of the crack surface except in the local region along the crack boundary where special crack-tip elements established by Rungamornrat and Mear (2008c) are employed to improve the approximation of $\Delta \mathbf{u}_j$ and the test function $\tilde{\mathbf{u}}_k$. Shape functions of those crack-tip elements are properly enriched by a square-root function to capture the right asymptotic behavior of $\Delta \mathbf{u}_j$. It is crucial to remark that the matrices \mathbf{C} and \mathbf{D} are essentially symmetric due to the symmetric integral form of \mathcal{C} and \mathcal{D} and the choice of basis functions used in the approximation, and that the matrix \mathbf{D}^* is not identical to \mathbf{D} owing to the application of special crack-tip elements to approximate

\tilde{u}_k in the local region near the crack front. Since both $\Sigma\mathbf{T}$ and $\Delta\mathbf{T}$ are known a priori, the unknown vector $\Delta\mathbf{U}$ is determined first by solving a symmetric system of linear algebraic equations (3.9) and subsequently $\Sigma\mathbf{U}$ is calculated from a symmetric system of linear algebraic equations (3.8).

3.3 NUMERICAL INTEGRATION SCHEME

While entries of the matrices \mathbf{D} and \mathbf{D}^* resulting from the single surface integrals with well-behavior integrands are accurately calculated by Gaussian quadrature, computation of the matrices \mathbf{U} and $\mathbf{C}, \mathbf{G}, \mathbf{H}$ clearly requires an extensive numerical evaluation of double surface integrals containing the kernels U_j^P and $C_{mj}^{iK}, G_{mj}^P, H_{ij}^P n_i$, respectively. Double surface integrals over a pair of elements with regular or well-behaved integrands are integrated efficiently using standard quadrature. In contrast, the double surface integrals with either nearly singular or weakly singular integrands resulting from a pair of identical or relatively close discretized elements cannot be integrated efficiently by standard quadrature rule (e.g., Xiao, 1998). Inaccurate evaluation of such integrals affects directly the quality of final numerical solutions. To circumvent such issue, special techniques based principally on suitable variable transformations reported in Li and Han (1985), Hayami and Brebbia (1988), Hayami (1992), Hayami and Matsumoto (1994) and Xiao (1998) are applied to either remove the weak singularity or regularize the rapid variation of integrands. After such regularization, standard quadrature rule can be exploited to efficiently integrate the resulting double surface integrals.

3.4 EFFICIENT EVALUATION OF KERNELS

Since the two-points kernel $H_{ij}^P(\boldsymbol{\xi} - \mathbf{y})$ is given in terms of elementary functions and the unit normal vector to the crack surface $n_i(\boldsymbol{\xi})$ or $n_i(\mathbf{y})$ can be computed using the geometry of discretized elements, the two kernels $H_{ij}^P(\boldsymbol{\xi} - \mathbf{y})n_i(\boldsymbol{\xi})$ and $H_{ik}^J(\boldsymbol{\xi} - \mathbf{y})n_i(\mathbf{y})$ can be evaluated directly in an efficient manner. In contrast, the two-points kernels $U_j^P(\boldsymbol{\xi} - \mathbf{y})$, $G_{mj}^P(\boldsymbol{\xi} - \mathbf{y})$ and $C_{mj}^{iK}(\boldsymbol{\xi} - \mathbf{y})$ for generally anisotropic, piezoelectric materials are given in terms of a closed contour integral for any pair of points $(\boldsymbol{\xi}, \mathbf{y})$ as shown in (2.11), (2.20) and (2.21). Although the involved line integral contains a well-behaved integrand, it is still computational inefficient to directly evaluate such integrals for all pairs of $(\boldsymbol{\xi}, \mathbf{y})$ resulting from the quadrature rule. In the present study, an interpolation-based approximation similar to that utilized by Rungamornrat and Mear (2008b, 2008c) is adopted to reduce the computational cost.

In particular, the closed contour integrals is evaluated numerically only one time using standard quadrature rule at all nodal points and values of all kernels at any pair of points (ξ, y) can be interpolated from the nodal values using selected element shape functions. The accuracy of this interpolation scheme can be improved by increasing the number of nodal points and orders of the interpolation functions.

3.5 CALCULATION OF GENERALIZED T-STRESS

Once the sum of the crack-face generalized displacement at all nodal points (ΣU) is determined, the generalized T-stress along the boundary of the crack is extracted from such information as described below.

Consider a crack-tip element located along the crack front where \mathbf{x}_c denotes a nodal point located at the crack boundary, $\{\mathbf{x}_c; x_1, x_2, x_3\}$ is a local reference Cartesian coordinate system with the origin \mathbf{x}_c and $\{\mathbf{e}_1, \mathbf{e}_2, \mathbf{e}_3\}$ denoting the corresponding base vectors as shown schematically in Figure 3.1. The generalized T-stresses contains five independent components denoted by T_{11} , T_{13} , T_{33} , T_{14} and T_{34} where the first three components are associated with the elastic T-stresses and the last two correspond to the electrical T-stresses. Values of the generalized T-stresses T_{11} , T_{13} , T_{33} , T_{14} and T_{34} at the point \mathbf{x}_c can be related to the finite part of the strain tensor and gradient of the electric potential at the point \mathbf{x}_c on the surface of a crack via the following constitutive relation

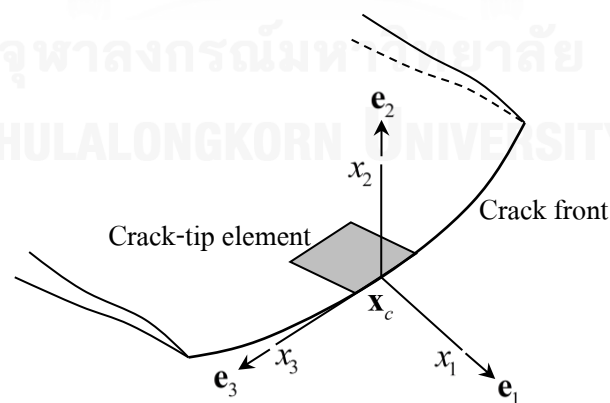


Figure 3.1 Schematic of crack-tip element and local coordinate system for calculation of generalized T-stress

$$T_{iJ} = E_{iJKl} \varepsilon_{Kl} \quad (3.10)$$

where the components T_{22} , T_{12} , T_{23} and T_{24} are known and equal to the prescribed generalized traction at a limiting point of the point \mathbf{x}_c on the crack surface. The components ε_{11} , ε_{13} , ε_{33} , ε_{41} and ε_{43} can be computed directly from the information of the sum of the generalized displacement in the neighborhood of the point \mathbf{x}_c via the following relations

$$\varepsilon_{11} = \frac{1}{2} \lim_{x \rightarrow x_c} \frac{\partial \Sigma u_1}{\partial x_1} = \frac{1}{2} \frac{\partial \Sigma u_1}{\partial x_1}(\mathbf{x}_c) \quad (3.11)$$

$$\varepsilon_{33} = \frac{1}{2} \lim_{x \rightarrow x_c} \frac{\partial \Sigma u_3}{\partial x_3} = \frac{1}{2} \frac{\partial \Sigma u_3}{\partial x_3}(\mathbf{x}_c) \quad (3.12)$$

$$\varepsilon_{13} = \frac{1}{4} \lim_{x \rightarrow x_c} \left\{ \frac{\partial \Sigma u_1}{\partial x_3} + \frac{\partial \Sigma u_3}{\partial x_1} \right\} = \frac{1}{4} \left\{ \frac{\partial \Sigma u_1}{\partial x_3} + \frac{\partial \Sigma u_3}{\partial x_1} \right\}(\mathbf{x}_c) \quad (3.13)$$

$$\varepsilon_{41} = \frac{1}{2} \lim_{x \rightarrow x_c} \frac{\partial \Sigma u_4}{\partial x_1} = \frac{1}{2} \frac{\partial \Sigma u_4}{\partial x_1}(\mathbf{x}_c) \quad (3.14)$$

$$\varepsilon_{43} = \frac{1}{2} \lim_{x \rightarrow x_c} \frac{\partial \Sigma u_4}{\partial x_3} = \frac{1}{2} \frac{\partial \Sigma u_4}{\partial x_3}(\mathbf{x}_c) \quad (3.15)$$

The derivatives involved in the expressions (3.11)-(3.15) can readily be computed within the crack-tip elements. By using the prescribed information of T_{22} , T_{12} , T_{23} and T_{24} and the computed components ε_{11} , ε_{13} , ε_{33} , ε_{41} and ε_{43} , the unknown strain components ε_{22} , ε_{12} , ε_{23} and ε_{42} and the generalized T-stresses T_{11} , T_{13} , T_{33} , T_{14} and T_{34} at the point \mathbf{x}_c can be determined from equation (3.10).

CHAPTER 4

NUMERICAL RESULTS AND DISCUSSIONS

To investigate the computational performance and accuracy of the proposed technique, extensive numerical experiments for various boundary value problems are conducted. Computed results for certain simple cases (e.g., a circular crack under simple electrical/mechanical loads) are benchmarked with available reference solutions to validate the formulation of governing integral equations and numerical implementations of the weakly singular SGBEM and the post-process for the generalized T-stress. Relatively complex problems such as non-planar cracks and multiple cracks are also considered to illustrate the capability, versatility, and robustness of the developed technique.

In the numerical study, a series of meshes with different levels of refinement are adopted and employed to investigate the convergence of computed numerical solutions. In particular, the majority of the crack surface is discretized by standard 6-nodes and 8-nodes, isoparametric elements whereas region adjacent to the crack boundary is discretized by 9-nodes special crack-tip elements. Linear piezoelectric materials selected in the analysis is transversely isotropic and all material constants are taken to be those of PZT-4 and PZT-5H as shown in Table 4.1.

Table 4.1 Generalized moduli of PZT-4 and PZT-5H (e.g., Li *et al.*, 2013; Rungamornrat and Mear, 2008c). The plan of isotropy is taken normal to the x_3 -axis.

		PZT-4	PZT-5H
Elastic constants ($\times 10^9$ Pa)	E_{1111}	139.00	126.00
	E_{1122}	77.80	55.00
	E_{1133}	74.30	53.00
	E_{3333}	113.00	117.00
	E_{1313}	25.60	35.30
Piezoelectric constants (C/m^2)	E_{1143}	-6.98	-6.50
	E_{3343}	13.80	23.30
	E_{1341}	13.40	17.00
Dielectric permittivities ($\times 10^{-9} C/(Vm)$)	$-E_{1441}$	6.00	15.10
	$-E_{3443}$	5.47	13.00

4.1 VERIFICATIONS

Let us consider a penny-shaped (circular) crack of radius a contained in a linear piezoelectric, infinite body with the poling direction along the x_3 -axis as shown in Figure 4.1. The crack is subjected to uniformly distributed pressure $t_3^+ = -t_3^- = \sigma_0$ and uniform distributed surface elastic charge $t_4^+ = -t_4^- = d_0$. This problem is chosen in the verification procedure since the complete mechanical/electrical fields are available in a closed form for an impermeable case (e.g., Chen *et al.*, 2000) and these results can be used to generate the benchmark solution for the generalized T-stress (see Appendix). Three meshes shown in Figure 4.2 are adopted in the analysis.

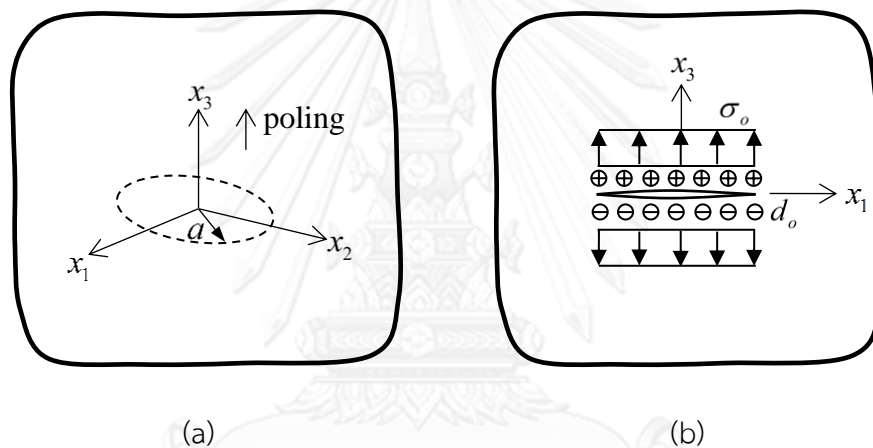


Figure 4.1 (a) Piezoelectric infinite body containing penny-shaped crack and (b) crack subjected to uniformly distributed pressure $t_3^+ = -t_3^- = \sigma_0$ and uniformly distributed surface electric charge $t_4^+ = -t_4^- = d_0$

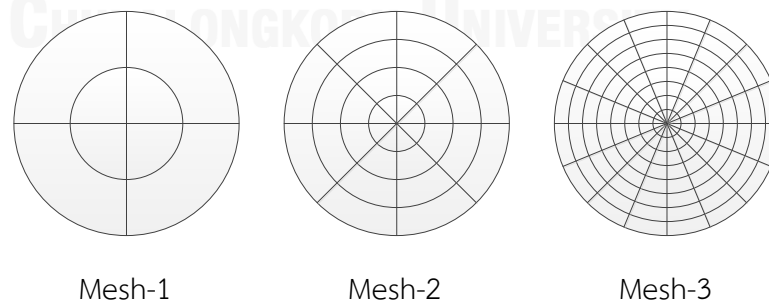


Figure 4.2 Three meshes of penny-shaped crack used in numerical study; Mesh-1 containing 8 elements and 4 crack-tip elements, Mesh-2 containing 32 elements and 8 crack-tip elements, and Mesh-3 containing 128 elements and 16 crack-tip elements

4.1.1 Piezoelectric material

For this particular problem, the generalized T-stress T_{11} and T_{33} are non-zero and are independent of positions along the crack front. The predicted results normalized by the analytical solution are shown in Tables 4.2 and 4.3 for both PZT-4 and PZT-5H and two loading cases: $\sigma_0=1\times 10^6 N/m^2$, $d_0=0$ and $\sigma_0=1\times 10^6 N/m^2$, $d_0=1\times 10^{-3} C/m^2$. It can be seen from these results that the computed T-stresses are in good agreement with the benchmark solution and, in addition, show weak dependence on meshes used. In particular, the errors of predicted solutions for all three meshes and two materials are less than 0.6% for the first loading case and less than 0.5% for the second loading case.

Table 4.2 Normalized generalized T-stress T_{11} for penny-shaped crack contained in piezoelectric unbounded medium under two loading cases

Mesh	$\frac{T_{11}}{T_{11}^{exact}}$			
	$\sigma_0=1\times 10^6 N/m^2$ $d_0=0$		$\sigma_0=1\times 10^6 N/m^2$ $d_0=1\times 10^{-3} C/m^2$	
	PZT-4	PZT-5H	PZT-4	PZT-5H
1	0.9954	0.9943	1.0050	0.9998
2	0.9968	0.9967	1.0036	1.0006
3	0.9953	0.9945	1.0019	1.0009

Table 4.3 Normalized generalized T-stress T_{33} for penny-shaped crack contained in piezoelectric unbounded medium under two loading cases

Mesh	$\frac{T_{33}}{T_{33}^{exact}}$			
	$\sigma_0=1\times 10^6 N/m^2$ $d_0=0$		$\sigma_0=1\times 10^6 N/m^2$ $d_0=1\times 10^{-3} C/m^2$	
	PZT-4	PZT-5H	PZT-4	PZT-5H
1	0.9954	0.9943	1.0050	0.9998
2	0.9968	0.9967	1.0036	1.0006
3	0.9953	0.9945	1.0019	1.0009

4.1.2 Isotropic and transversely isotropic material

As an additional verification, let us consider a special case when the constituting material is simply linear elastic and the medium is subjected only to the uniform normal traction. For this particular case, the reference solution for the T-stress can be obtained from Wang (2004) for the isotropic case and post-processed from the stress field presented by Fabrikant (1989) for the transversely isotropic case. In the numerical study, the piezoelectric constants are input equal to zero whereas the elastic moduli are taken as shown in Table 4.4. The numerical results for non-zero T-stress components normalized by the analytical solution are reported in Table 4.5. Clearly, the good agreement between computed solutions and the benchmark solution is observed; for all three meshes, the discrepancy is less than 0.34% and 0.64% for isotropic and transversely isotropic materials, respectively.

Table 4.4 Elastic constants for isotropic and transversely isotropic materials used in the analysis

		Isotropic	Transversely isotropic
Elastic constants ($\times 10^9$ Pa)	E_{1111}	1.35	126.00
	E_{1122}	0.58	55.00
	E_{1133}	0.58	53.00
	E_{3333}	1.35	117.00
	E_{1313}	0.38	35.30

Table 4.5 Normalized T-stress T_{11} and T_{33} of penny-shaped crack embedded in isotropic and transversely isotropic, linear elastic, infinite medium under uniform normal traction

Mesh	$\frac{T_{11}}{T_{11}^{exact}}$		$\frac{T_{33}}{T_{33}^{exact}}$	
	Isotropic	Transversely isotropic	Isotropic	Transversely isotropic
1	0.9966	1.0063	1.0020	1.019
2	0.9984	1.0025	0.9998	1.0039
3	0.9966	1.0008	0.9997	1.0038

4.2 MORE COMPLEX BOUNDARY VALUE PROBLEMS

After the proposed technique is verified, various crack problems are investigated. Results for representative cases are presented here to demonstrate its capability and robustness to treat planar cracks of general geometry, non-flat cracks, and multiple cracks. Since boundary value problems considered here are quite complex, analytical solution for all cases in this particular section does not exist and, as a result, only the convergence test using three different levels of meshes is performed.

4.2.1 Tunnel crack

Consider a tunnel crack with a half-length L and end radius R contained in a linear piezoelectric infinite body as shown in Figure 4.3(a). The crack surface is oriented normal the poling direction and the axis of material symmetry. Similar to the previous problem, the crack is subjected to uniformly distributed pressure $t_3^+ = -t_3^- = \sigma_0$ and uniformly distributed surface electric charge $t_4^+ = -t_4^- = d_0$ as depicted in Figure 4.3(c). In the numerical study, three meshes adopted as shown in Figure 4.4 and two materials (i.e., PZT-4 and PZT-5H) indicated in Table 4.1 are considered to examine the convergence behavior of predicted solutions.

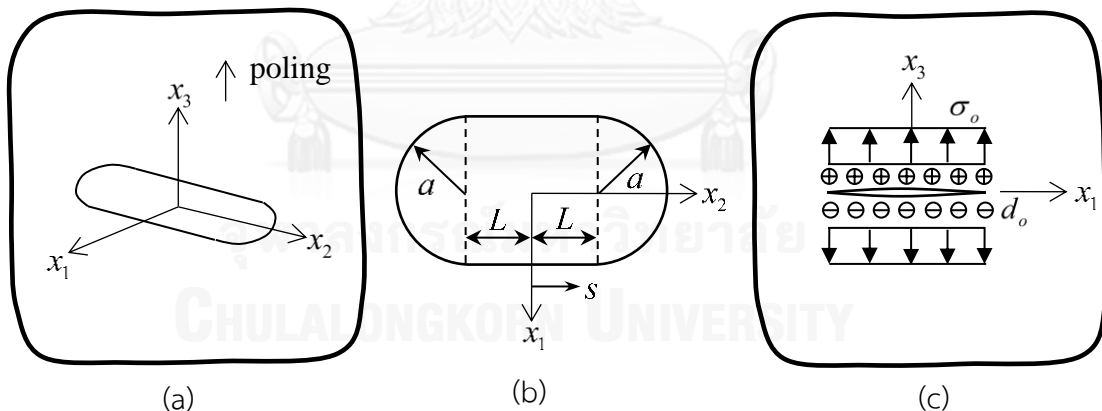


Figure 4.3 (a) Schematic of infinite piezoelectric medium containing tunnel crack in x_1-x_2 plane, (b) geometry of tunnel crack, and (c) tunnel crack subjected to uniform pressure $t_3^+ = -t_3^- = \sigma_0$ and uniform electric charge $t_4^+ = -t_4^- = d_0$

The same two loading cases as the previous problem are considered. For the pure mechanical loading (i.e., $\sigma_0 = 1 \times 10^6 \text{ N/m}^2$ and $d_0 = 0$), the computed non-zero generalized T-stress, T_{11} , T_{13} and T_{33} , obtained from the three meshes reported in

Figures 4.5 and 4.6 for PZT-4 and PZT-5H, respectively. Results for the mixed mechanical/electrical loading (i.e., $\sigma_0 = 1 \times 10^6 \text{ N/m}^2$ and $d_0 = 1 \times 10^{-3} \text{ C/m}^2$) are shown in Figures 4.7 and 4.8 for PZT-4 and PZT-5H, respectively. It is seen, again, that the computed generalized T-stresses show good convergence characteristics for all cases. In addition, the coarsest mesh with significantly large elements along the crack front can yield results comparable to those from the fine mesh. This should be due to the discretization of a local region adjacent to the crack front by special crack-tip elements to accurately model the near-tip crack-face data.

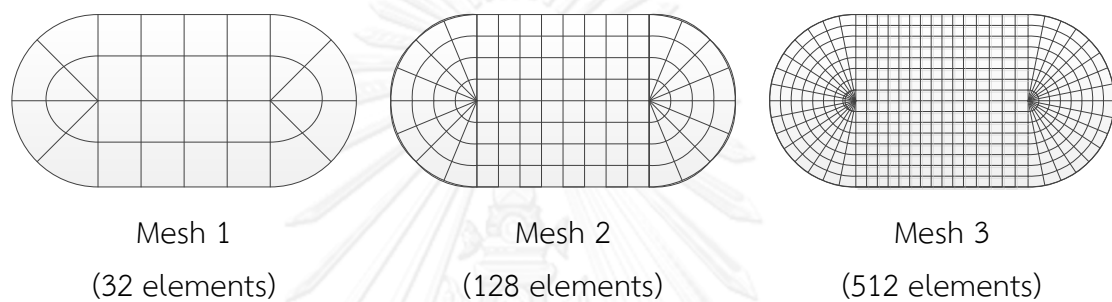


Figure 4.4 Three meshes of tunnel crack used in numerical study; Mesh-1 containing 32 elements with 16 crack-tip elements, Mesh-2 containing 128 elements with 32 crack-tip elements, and Mesh-3 containing 512 elements with 64 crack-tip elements

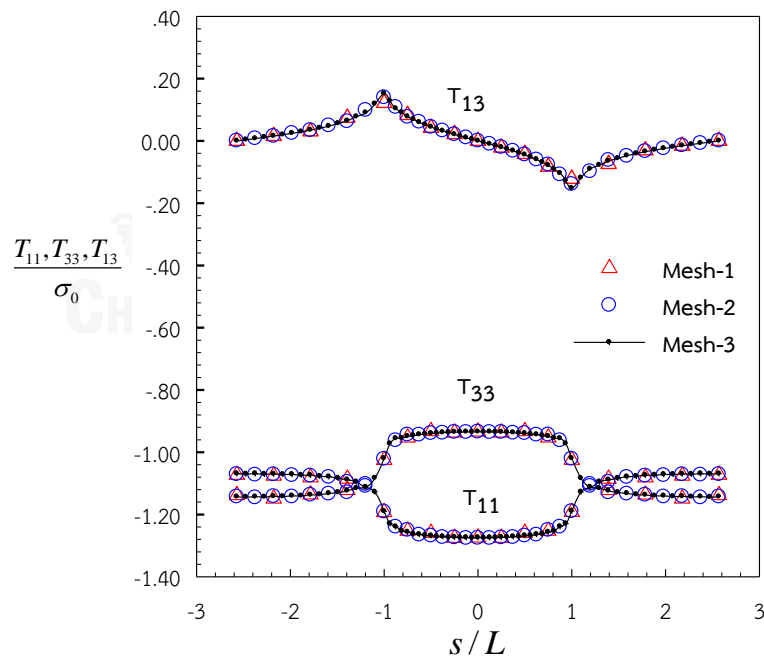


Figure 4.5 Normalized non-zero generalized T-stress of tunnel crack in PZT-4 under $\sigma_0 = 1 \times 10^6 \text{ N/m}^2$ and $d_0 = 0$

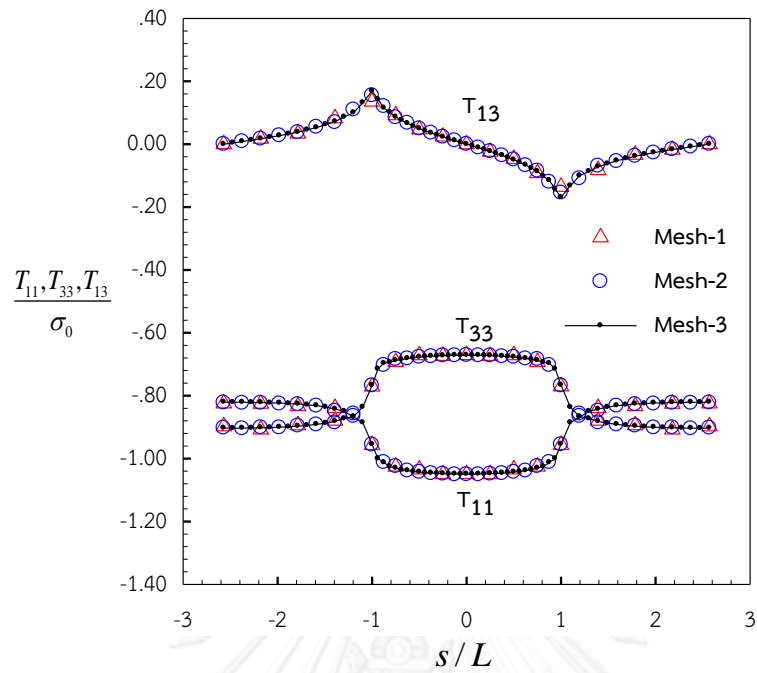


Figure 4.6 Normalized non-zero generalized T-stress of tunnel crack in PZT-5H under $\sigma_0 = 1 \times 10^6 \text{ N/m}^2$ and $d_0 = 0$

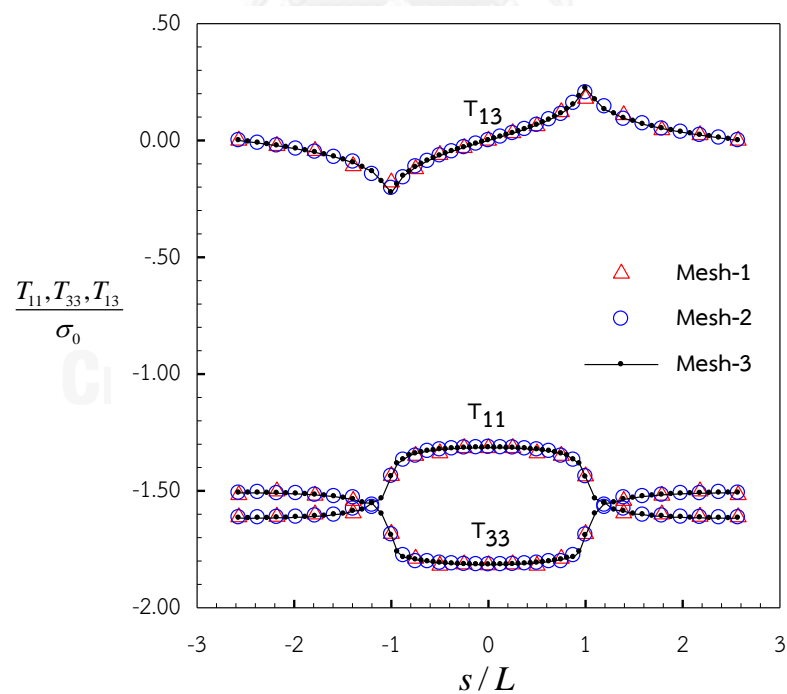


Figure 4.7 Normalized non-zero generalized T-stress of tunnel crack in PZT-4 under $\sigma_0 = 1 \times 10^6 \text{ N/m}^2$ and $d_0 = 1 \times 10^{-3} \text{ C/m}^2$

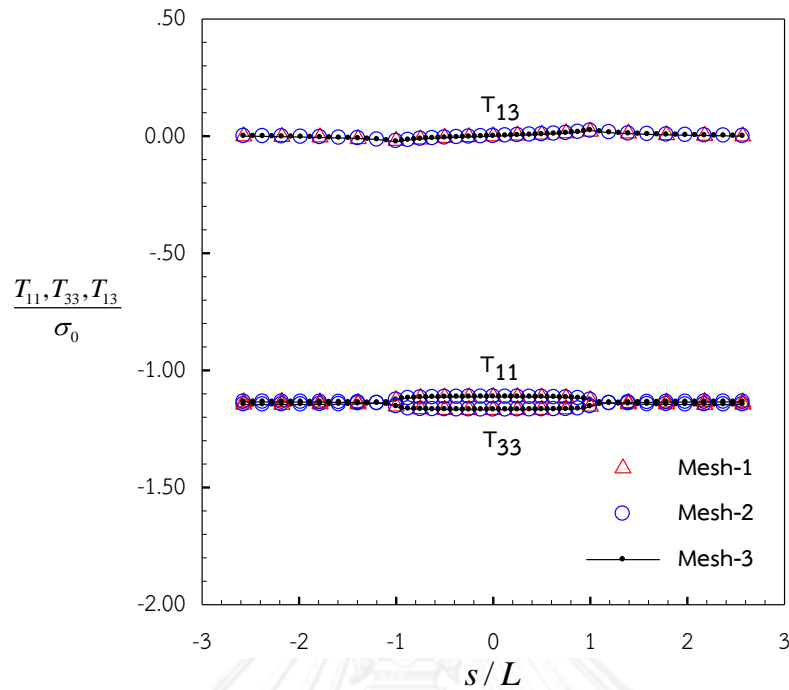


Figure 4.8 Normalized non-zero generalized T-stress of tunnel crack in PZT-5H under $\sigma_0 = 1 \times 10^6 \text{ N/m}^2$ and $d_0 = 1 \times 10^{-3} \text{ C/m}^2$

To demonstrate the influence of the ratio L/a on the distribution of the generalized T-stress along boundary of the crack, three values of the half-length $L = a$, $5a$ and $10a$ are considered. Due to the good convergence behavior of the numerical solutions indicated above, the level of refinement equivalent to the mesh-2 shown in Figure 4.4 for $L = a$ is utilized throughout. The generalized T-stress T_{11} along straight portion of the crack front is illustrated in Figure 4.9 and Figure 4.10 for the crack under uniformly distributed pressure $t_3^+ = -t_3^- = \sigma_0$ and uniformly distributed surface electric charge $t_4^+ = -t_4^- = d_0$, respectively. The analytical solutions for the plane strain case proposed by Hao and Biao (2004) for the straight crack of length $2a$ under the same loading conditions are also shown in the plots. It can be seen from this set of results that as L/a increases the value of the generalized T-stress is almost constant along the straight portion of the crack front and tends to approach the plane strain solution.

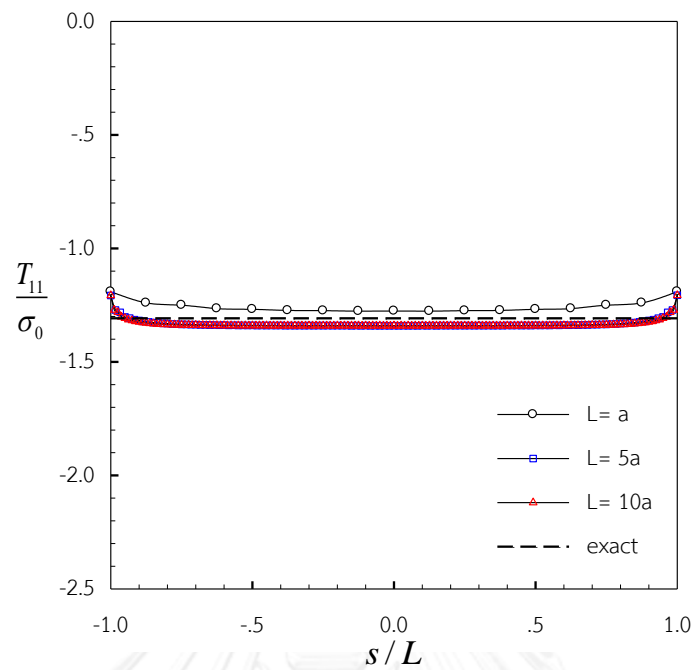


Figure 4.9 Normalized T_{11}/σ_0 of extended tunnel crack to plane strain problem in PZT-4 under $\sigma_0 = 1 \times 10^6 \text{ N/m}^2$

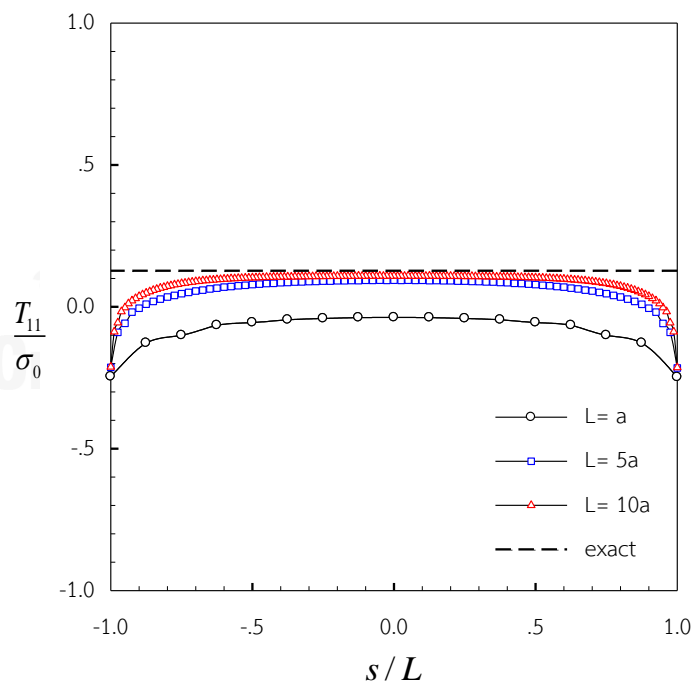


Figure 4.10 Normalized T_{11}/σ_0 of extended tunnel crack to plane strain problem in PZT-4 under $\sigma_0 = 1 \times 10^6 \text{ N/m}^2$

4.2.2 Spherical cap crack

To further demonstrate the ability of the current technique to solve non-flat cracks, let us consider a representative problem associated with a transversely isotropic, linear piezoelectric, infinite body containing a spherical cap crack as depicted in Figure 4.11. The surface of a crack is defined by

$$x_1 = a \sin \gamma \cos \beta, \quad x_2 = a \sin \gamma \sin \beta, \quad x_3 = a \cos \gamma \quad (4.1)$$

where (x_1, x_2, x_3) are coordinates of any point on the crack; a denotes the spherical crack radius; $\beta \in [0, 2\pi]$; and $\gamma \in [0, \theta]$ with θ denoting the half subtended angle of the spherical surface. The medium is subjected to three loading cases: (i) the uniform remote tension $\sigma_{33}^\infty = \sigma_0$ (see Figure 4.12(a)), (ii) the uniform remote biaxial tension $\sigma_{11}^\infty = \sigma_{33}^\infty = \sigma_0$ (see Figure 4.12(b)), and (iii) the uniform remote tension $\sigma_{33}^\infty = \sigma_0$ and uniform remote electric induction $\sigma_{34}^\infty = d_0$ (see Figure 4.12(c)). The poling direction and the axis material symmetry are coincident with the x_3 -axis. In the numerical study, the half subtended angle $\theta = 45^\circ$ and two materials PZT-4 and PZT-5H are chosen and three meshes as shown in Figure 4.13 are adopted.

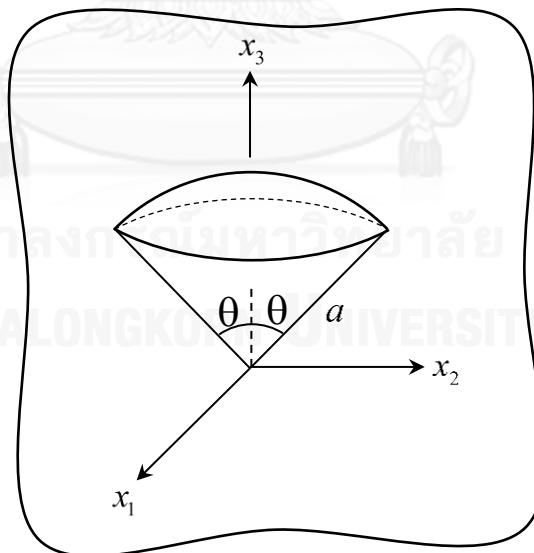


Figure 4.11 A linear piezoelectric, infinite body containing spherical cap crack

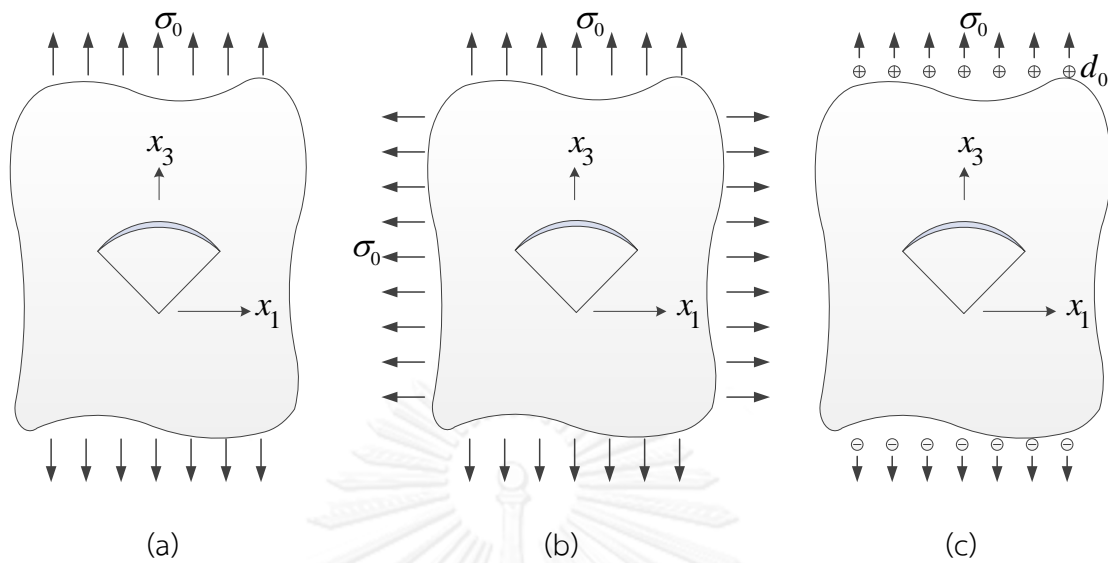


Figure 4.12 Spherical cap crack subjected to (a) uniform remote tension $\sigma_{33}^{\infty} = \sigma_0$, (b) uniform remote biaxial tension $\sigma_{11}^{\infty} = \sigma_{33}^{\infty} = \sigma_0$, and (c) uniform remote tension $\sigma_{33}^{\infty} = \sigma_0$ and uniform remote electric induction $\sigma_{34}^{\infty} = d_0$

4.2.2.1 Uniform remote tension

For this particular load case, the non-zero generalized T-stresses T_{11} , T_{33} and T_{14} are all independent of positions along the crack front due to the axisymmetry. The computed numerical results normalized properly by the benchmark solution (taken from the results of the Mesh-3) are shown in Tables 4.6-4.8 for $\sigma_0 = 1 \times 10^6 \text{ N/m}^2$. It can be seen that the generalized T-stresses obtained from all meshes are in good agreement. In particular, the discrepancy between solutions generated by the coarse and intermediate meshes and that of the fine mesh is less than 2.0 % and 0.2 % for T_{11} , 0.9 % and 0.2 % for T_{33} , and 2.3 % and 0.4 % for T_{14} , respectively.

4.2.2.2 Uniform remote biaxial tension

For this load case, non-zero generalized T-stresses T_{11} , T_{33} , T_{13} , T_{14} and T_{34} vary as a function of positions along the boundary of the crack. The numerical results for the generalized are obtained for $\sigma_0 = 1 \times 10^6 \text{ N/m}^2$ and then reported versus the angle β in Figures 4.14 and 4.15 for PZT-4 and in Figures 4.16 and 4.17 for PZT-5H. Again, the obtained numerical solutions indicate the good convergence behavior. The computed generalized T-stresses predicted by the coarsest mesh deviate slightly from solutions of the finest mesh whereas the intermediate and finest meshes yield

nearly identical solutions. As an additional remark, values of the generalized T-stress show strong dependent on the material properties; for instance, values of T_{11} and T_{33} for PZT-4 are quite different whereas they are almost identical for PZT-5H.

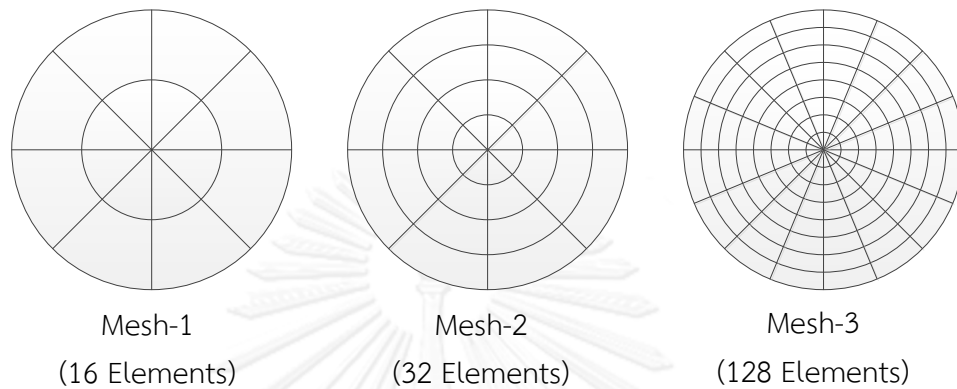


Figure 4.13 Meshes of spherical cap crack used in analysis (schematics only show projected meshes on the $x_1 - x_2$ plane); Mesh-1 containing 16 elements with 8 crack-tip elements, Mesh-2 containing 32 elements with 8 crack-tip elements, and Mesh-3 containing 128 elements with 16 crack-tip elements

Table 4.6 Normalized generalized T-stress T_{11} for spherical cap crack in linear piezoelectric infinite body under (i) uniform remote tension $\sigma_0 = 1 \times 10^6 \text{ N/m}^2$ and (ii) uniform remote tension $\sigma_0 = 1 \times 10^6 \text{ N/m}^2$ and uniform remote electric induction $d_0 = 1 \times 10^{-3} \text{ C/m}^2$

Mesh	$\frac{T_{11}}{T_{11}^{ref}}$			
	$\sigma_0 = 1 \times 10^6 \text{ N/m}^2$		$\sigma_0 = 1 \times 10^6 \text{ N/m}^2$ $d_0 = 1 \times 10^{-3} \text{ C/m}^2$	
	PZT-4	PZT-5H	PZT-4	PZT-5H
1	0.9803	0.9864	0.9739	0.9791
2	0.9987	0.9990	0.9937	0.9958
3	1.0000	1.0000	1.0000	1.0000

Table 4.7 Normalized generalized T-stress T_{33} for spherical cap crack in linear piezoelectric infinite body under (i) uniform remote tension $\sigma_0 = 1 \times 10^6 \text{ N/m}^2$ and (ii) uniform remote tension $\sigma_0 = 1 \times 10^6 \text{ N/m}^2$ and uniform remote electric induction $d_0 = 1 \times 10^{-3} \text{ C/m}^2$

Mesh	T_{33} / T_{33}^{ref}			
	$\sigma_0 = 1 \times 10^6 \text{ N/m}^2$		$\sigma_0 = 1 \times 10^6 \text{ N/m}^2$ $d_0 = 1 \times 10^{-3} \text{ C/m}^2$	
	PZT-4	PZT-5H	PZT-4	PZT-5H
1	0.9919	0.9952	0.9817	0.9924
2	0.9987	0.9990	0.9971	0.9986
3	1.0000	1.0000	1.0000	1.0000

Table 4.8 Normalized generalized T-stress T_{14} for spherical cap crack in linear piezoelectric infinite body under (i) uniform remote tension $\sigma_0 = 1 \times 10^6 \text{ N/m}^2$ and (ii) uniform remote tension $\sigma_0 = 1 \times 10^6 \text{ N/m}^2$ and uniform remote electric induction $d_0 = 1 \times 10^{-3} \text{ C/m}^2$

Mesh	T_{14} / T_{14}^{ref}			
	$\sigma_0 = 1 \times 10^6 \text{ N/m}^2$		$\sigma_0 = 1 \times 10^6 \text{ N/m}^2$ $d_0 = 1 \times 10^{-3} \text{ C/m}^2$	
	PZT-4	PZT-5H	PZT-4	PZT-5H
1	0.9779	0.9868	0.9755	0.9829
2	0.9964	0.9981	0.9938	0.9963
3	1.0000	1.0000	1.0000	1.0000

4.2.2.3 Uniform remote tension and surface electric charge

The final load case is axisymmetric and, as a result, only the generalized T-stresses T_{11} , T_{33} and T_{14} are non-zero and are independent of positions along the crack front. The obtained numerical results compared with the reference solution (taken from the results of the Mesh-3) are reported in Tables 4.6-4.8 for $\sigma_0 = 1 \times 10^6 \text{ N/m}^2$ and $d_0 = 1 \times 10^{-3} \text{ C/m}^2$. Similar to the above two load cases that converged solutions can be obtained. In particular, the discrepancy between solutions generated by the coarse and intermediate meshes and that of the fine mesh is less than 2.7 % and 0.7 % for T_{11} , 1.9 % and 0.3 % for T_{33} , and 2.6 % and 0.7 % for T_{14} , respectively.

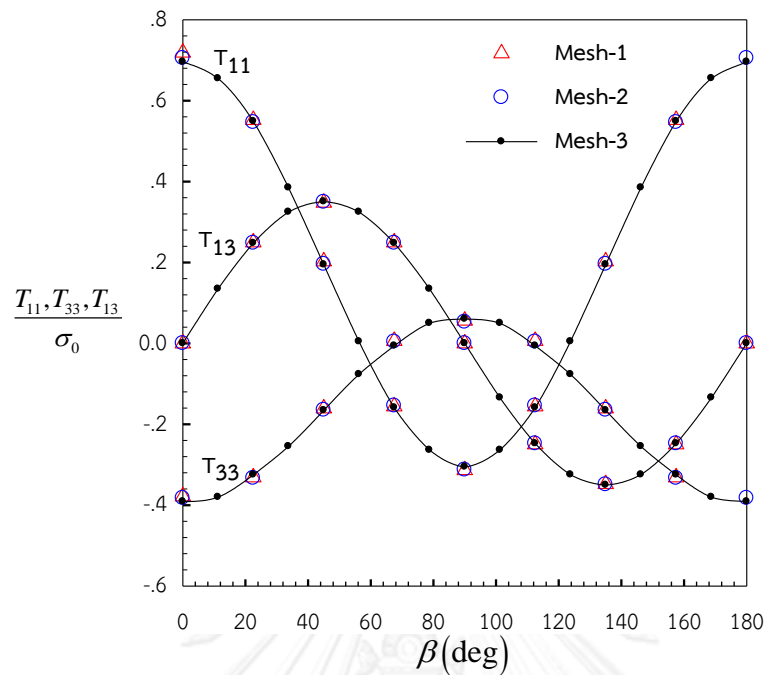


Figure 4.14 Normalized T_{11}/σ_0 , T_{33}/σ_0 and T_{13}/σ_0 for spherical cap crack subjected to uniform remote biaxial tension $\sigma_0 = 1 \times 10^6 \text{ N/m}^2$. Results are reported for PZT-4.

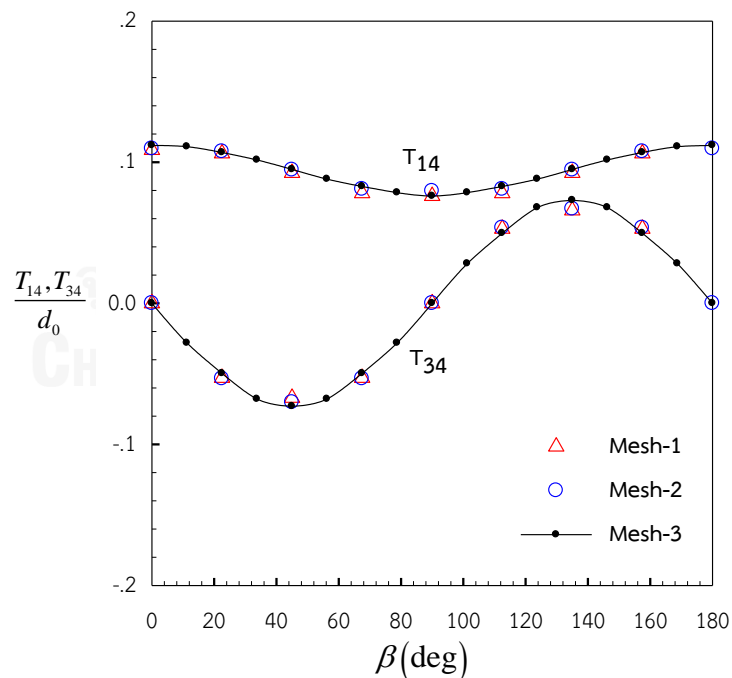


Figure 4.15 Normalized T_{14}/d_0 and T_{34}/d_0 for spherical cap crack subjected to uniform remote biaxial tension $\sigma_0 = 1 \times 10^6 \text{ N/m}^2$. Results are reported for PZT-4.

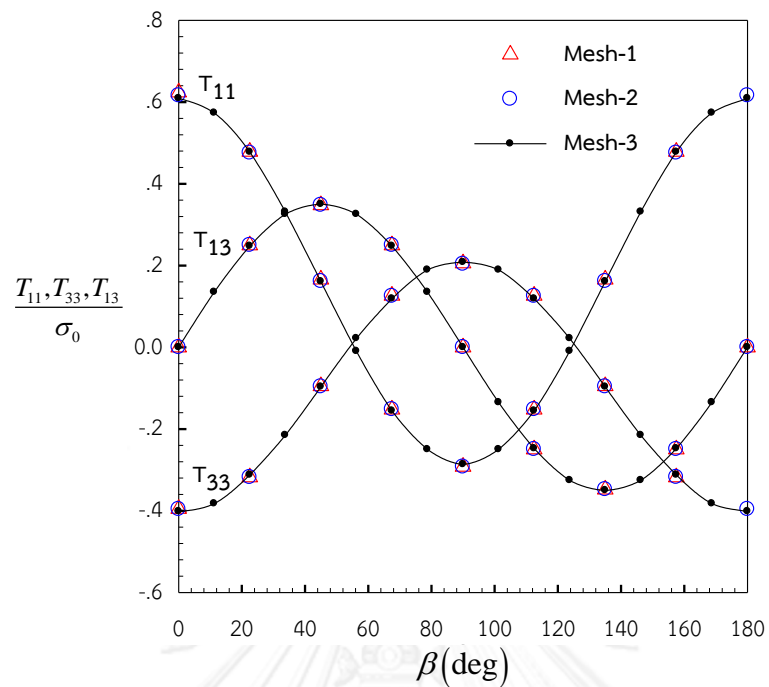


Figure 4.16 Normalized T_{11}/σ_0 , T_{33}/σ_0 and T_{13}/σ_0 for spherical cap crack subjected to uniform remote biaxial tension $\sigma_0=1\times 10^6 N/m^2$. Results are reported for PZT-5H.

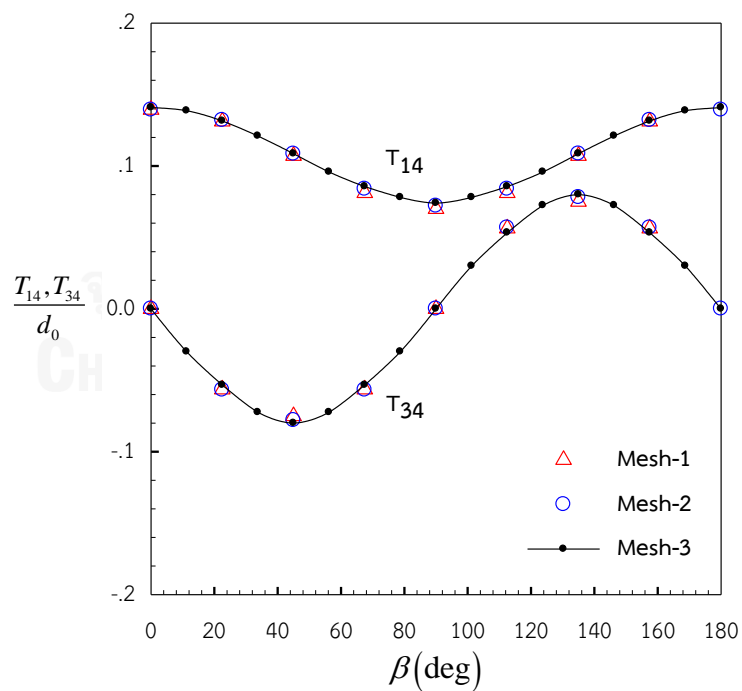


Figure 4.17 Normalized T_{14}/d_0 and T_{34}/d_0 for spherical cap crack subjected to uniform remote biaxial tension $\sigma_0=1\times 10^6 N/m^2$. Results are reported for PZT-5H.

4.2.3 Pair of penny-shaped cracks

Finally, the ability of the developed technique to treat multiple cracks is explored. A representative problem associated with a pair of identical co-planar circular cracks of radius a contained in a transversely isotropic, linear piezoelectric infinite body under a uniform remote tension $\sigma_{33}^{\infty} = \sigma_0$ as indicated in Figure 4.18 is considered. The crack fronts of both cracks, termed crack-A and crack-B, are defined by

$$\text{crack-A: } x_1 = a \sin \beta, \quad x_2 = d + a \cos \beta, \quad x_3 = 0 \quad (4.2)$$

$$\text{crack-B: } x_1 = a \sin \beta, \quad x_2 = -d + a \cos \beta, \quad x_3 = 0 \quad (4.3)$$

where $\beta \in [0, 2\pi]$ and $2d$ denotes the distance between the centers of the two cracks. The crack surface is oriented perpendicular to the poling direction and the material symmetry axis (i.e., perpendicular to the x_3 -axis). In numerical experiments, the distance $d = 1.125a$, two material models PZT-4 and PZT-5H, and $\sigma_0 = 1 \times 10^6 \text{ N/m}^2$ are employed. Three meshes adopted as shown in Figure 4.19 are used to investigate the convergence behavior of predicted results.

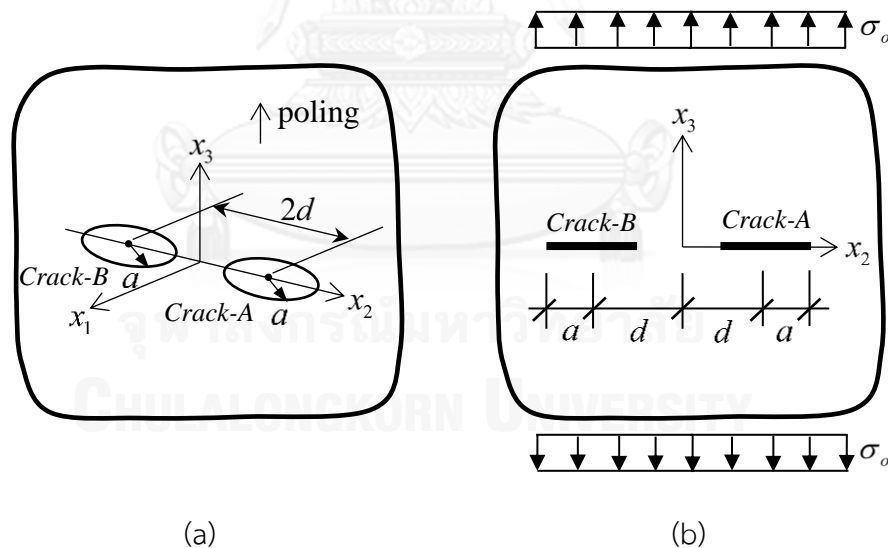


Figure 4.18 (a) A pair of identical co-planar circular cracks in transversely isotropic, linear piezoelectric, infinite domain and (b) body under uniform remote tension $\sigma_{33}^{\infty} = \sigma_0$

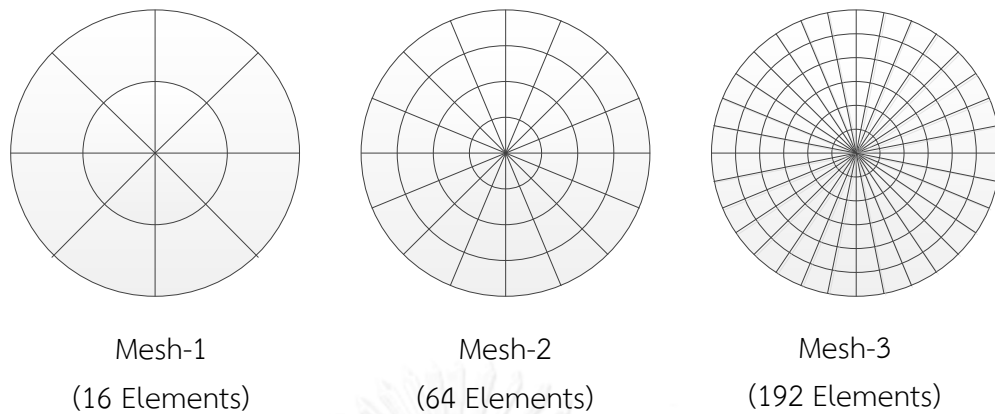


Figure 4.19 Three meshes of penny-shaped crack used in numerical study; Mesh-1 containing 16 elements with 8 crack-tip elements, Mesh-2 containing 64 elements with 16 crack-tip elements, and Mesh-3 containing 192 elements with 32 crack-tip elements

Numerical results for the generalized T-stress T_{11} , T_{33} and T_{13} for the *crack-B* obtained from the three meshes are properly normalized and reported versus the angular position in Figures 4.20-4-22 for PZT-4 and PZT-5H. It is seen again from obtained results that solutions predicted by all meshes indicate the good agreement; results from the Mesh-3 are very close to those from the Mesh-2 but slightly different from those from the Mesh-1.

To additionally explore the effect of the distance between the two circular cracks on the values of generalized T-stresses, various values of d ranging from $1.125a$ to $1.5a$ are considered. Numerical results for the generalized T-stresses T_{11} , T_{33} and T_{13} for the *crack-B* obtained from the Mesh-3 are properly normalized and then reported in Figures 4.23-4-26 for PZT-4 and PZT-5H. The exact solution of an isolated penny-shaped crack under the same loading condition is also included in the plots. It is evident that the interaction of the two cracks is more significant when d/a is close to 1 and it generally renders the generalized T-stresses non-uniform along the crack front. Clearly, more rapid variation of the generalized T-stress in the region where the crack fronts of the two cracks are relatively close is observed.

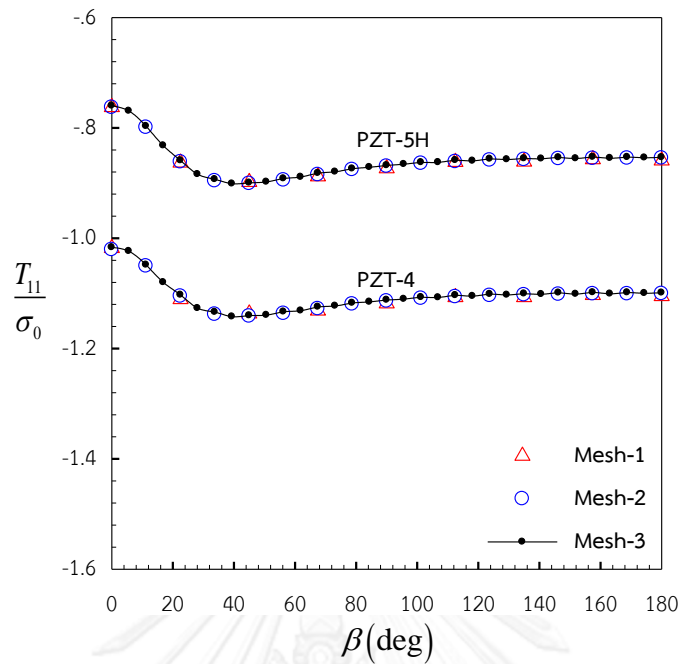


Figure 4.20 Normalized T_{11} for *Crack-B* in a pair of two identical co-planar circular cracks in linear piezoelectric infinite body under uniform remote tension $\sigma_0 = 1 \times 10^6 \text{ N/m}^2$. Results are reported for PZT-4 and PZT-5H.

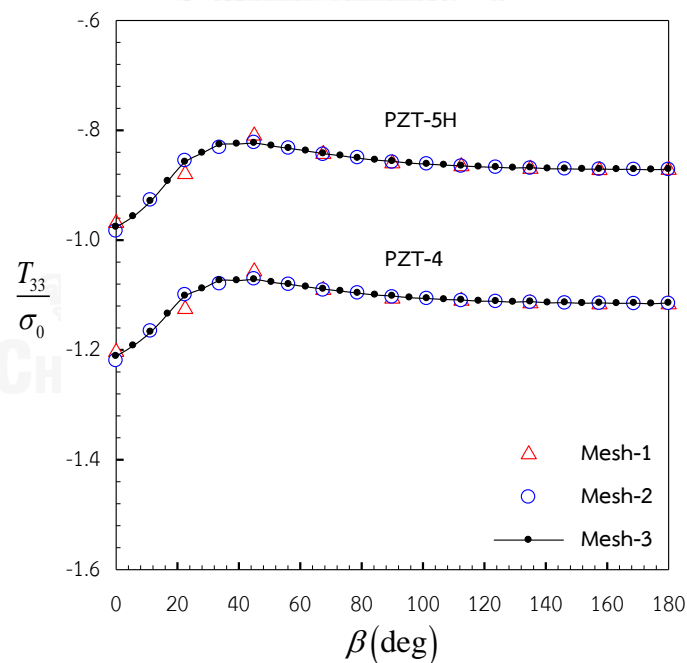


Figure 4.21 Normalized T_{33} for *Crack-B* in a pair of two identical co-planar circular cracks in linear piezoelectric infinite body under uniform remote tension $\sigma_0 = 1 \times 10^6 \text{ N/m}^2$. Results are reported for PZT-4 and PZT-5H.

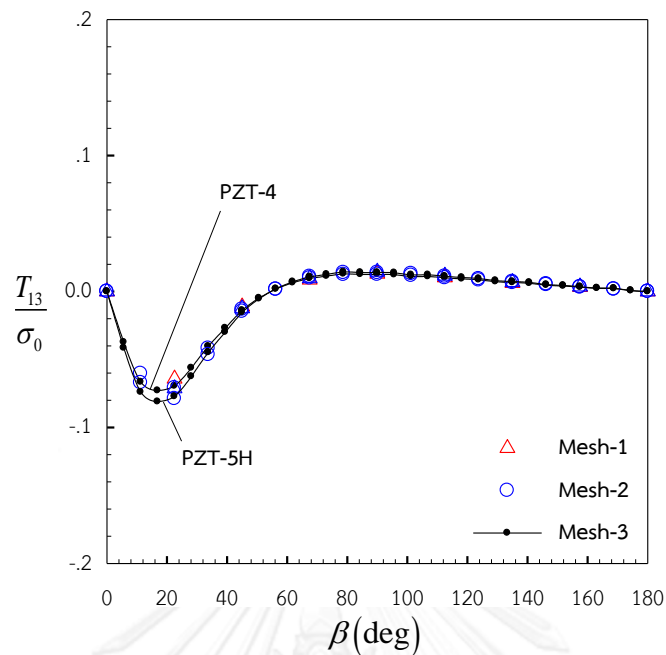


Figure 4.22 Normalized T_{13} for *Crack-B* in a pair of two identical co-planar circular cracks in linear piezoelectric infinite body under uniform remote tension $\sigma_0 = 1 \times 10^6 \text{ N/m}^2$. Results are reported for PZT-4.

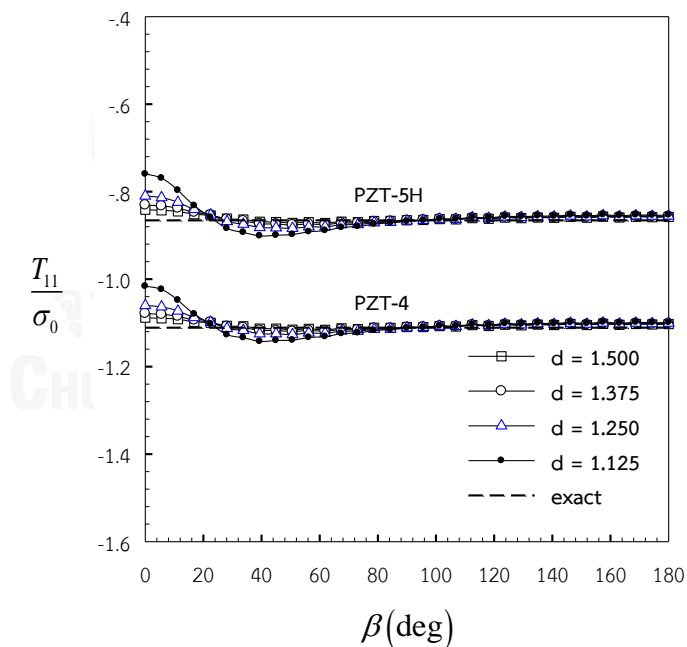


Figure 4.23 Normalized T_{11} for *Crack-B* in a pair of two identical co-planar circular cracks in linear piezoelectric infinite body under uniform remote tension $\sigma_0 = 1 \times 10^6 \text{ N/m}^2$. Varies distance between cracks. Results are reported for PZT-4 and PZT-5H.

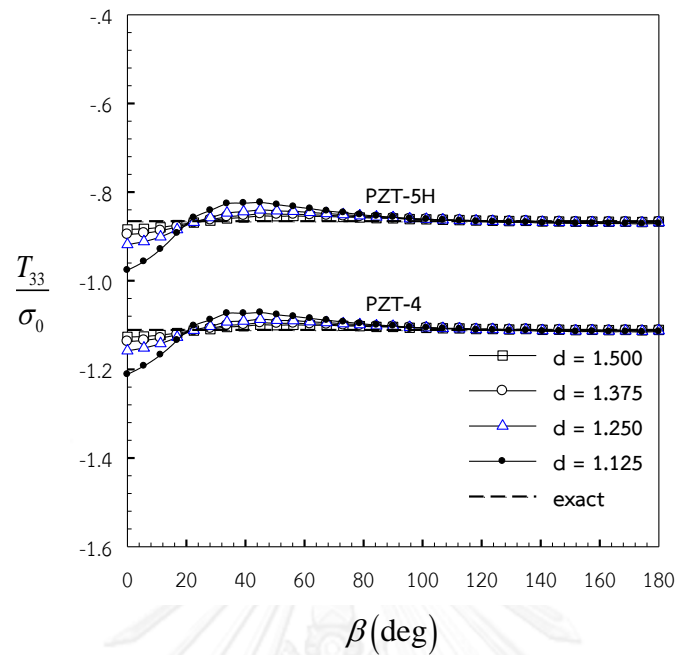


Figure 4.24 Normalized T_{33} for *Crack-B* in a pair of two identical co-planar circular cracks in linear piezoelectric infinite body under uniform remote tension $\sigma_0 = 1 \times 10^6 \text{ N/m}^2$. Varies distance between cracks. Results are reported for PZT-4 and PZT-5H.

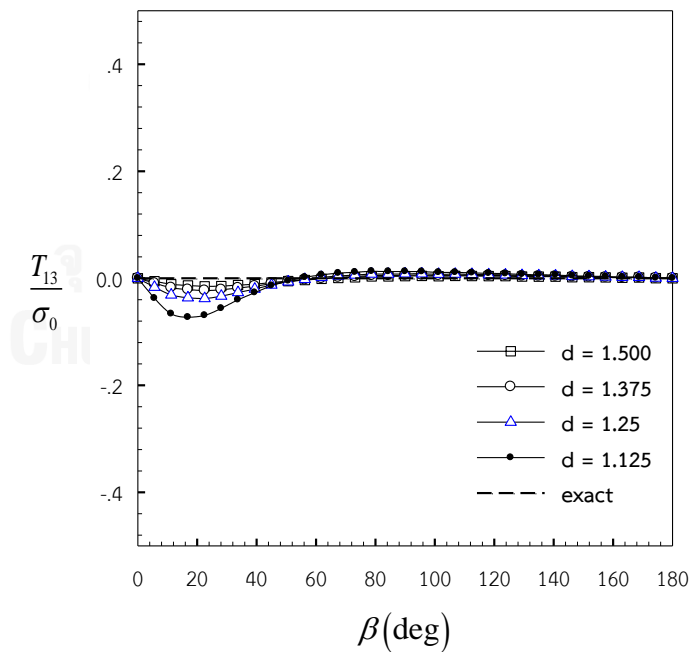


Figure 4.25 Normalized T_{13} for *Crack-B* in a pair of two identical co-planar circular cracks in linear piezoelectric infinite body under uniform remote tension $\sigma_0 = 1 \times 10^6 \text{ N/m}^2$. Varies distance between cracks. Results are reported for PZT-4.

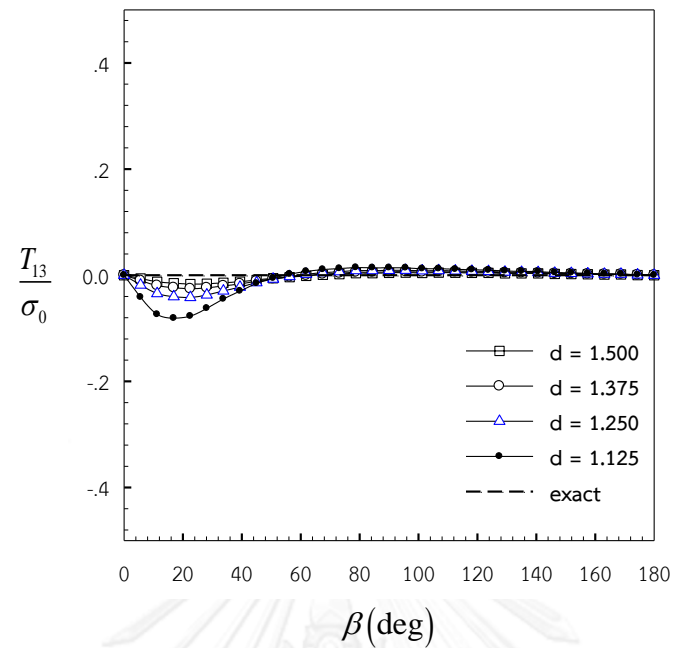


Figure 4.26 Normalized T_{13} for *Crack-B* in a pair of two identical co-planar circular cracks in linear piezoelectric infinite body under uniform remote tension $\sigma_0 = 1 \times 10^6 \text{ N/m}^2$. Varies distance between cracks. Results are reported for PZT-5H.

CHAPTER 5

CONCLUSIONS AND REMARKS

An efficient and accurate numerical procedure based primarily on the weakly singular boundary integral equation method has been successfully implemented for determining the generalized T-stresses of impermeable cracks in a three-dimensional, linear piezoelectric, infinite body. The technique has been established in a general context allowing both planar and non-planar cracks under arbitrarily distributed applied traction being treated. The completely regularized boundary integral equations for both the generalized displacements and generalized tractions have been used. This particular pair of boundary integral equations involves only weakly singular kernels allowing the interpretation of their values in the sense of Riemann and, in addition, requiring only continuous crack-face data for their validity. To solve the boundary integral equation for the generalized traction, the weakly singular symmetric Galerkin boundary element method (SGBEM) has been implemented to compute relative crack-face generalized displacements. To improve the computational efficiency, all involved kernels for generally anisotropic materials have been evaluated using the interpolation technique to reduce the massive calculations associated with the direct evaluation of line integrals. In addition, weakly singular integrals and nearly singular integrals resulting directly from the discretization have been evaluated numerically using a selected special quadrature scheme. Once all unknown functions on the surface of the crack have been solved, the generalized T-stresses have been post-processed using the information of the gradient of the sum of the generalized displacement along the crack front.

From an extensive numerical study of various scenarios, the proposed technique has been found accurate, efficient, and robust for the analysis of the generalized T-stress of cracks in linear piezoelectric infinite bodies. The verification procedure via existing benchmark solutions has confirmed both the formulation and the implementation of the proposed technique. By using special elements along the crack boundary to model the near-tip relative crack-face generalized displacement, reasonably accurate results can be obtained using relatively coarse meshes. The capability of the proposed technique to model arbitrary shaped cracks (e.g., non-planar cracks) and multiple cracks should be beneficial, as a computational tool, for performing full three-dimensional, piezoelectric fracture analysis.

As a final remark, while the numerical technique has been implemented successfully and proved to yield highly accurate results for the generalized T-stress, the formulation and implementation are still restricted to impermeable cracks in infinite media. Extensions of the present development to treat cracks in a finite body and more complex boundary conditions such as semi-permeable and Landis-type models should be potentially useful since it enhances the capability of the developed technique to solve a larger class of boundary value problems. In addition, the current study focused primarily on the development of the computational procedure but use of the developed tool to explore the behavior and influence of various parameters on the generalized T-stress is still not complete and requires further investigation.



REFERENCES

- Chen, M. C. 2003a. Application of finite-part integrals to the three-dimensional fracture problems for piezoelectric media, Part I: hypersingular integral equation and theoretical analysis. Int. J. Fract. 121: 133-148.
- Chen, M. C. 2003b. Application of finite-part integrals to the three-dimensional fracture problems for piezoelectric media, Part II: numerical analysis. Int. J. Fract. 121: 149-161.
- Chen, W. Q., and Lim, C. W. 2005. 3D point force solution for a permeable penny-shaped crack embedded in an infinite transversely isotropic piezoelectric medium. International Journal of Fracture 131: 231-246.
- Chen, W. Q., and Shioya, T. 2000. Complete and exact solutions of a penny-shaped crack in a piezoelectric solid: antisymmetric shear loadings. International Journal of Solids and Structures 37: 2603-2619.
- Chen, W. Q., Shioya, T., and Ding, H. J. 2000. A penny-shaped crack in piezoelectrics : resolved. International Journal of Fracture 105: 49-56.
- Cotterell, B., and Rice, J. R. 1980. Slightly curved or kinked cracks. International Journal of Fracture 16.
- Davi, G., and Milazzo, A. 2001. Multidomain boundary integral formulation for piezoelectric materials fracture mechanics. Int. J. Solids Struct. 38: 7065-7078.
- Deeg, W. F. 1980. The analysis of dislocation, crack and inclusion problems in piezoelectric solids. Doctoral dissertation, Department of Materials Science and Engineering, Stanford University.
- Groh, U., and Kuna, M. 2005. Efficient boundary element analysis of cracks in 2D piezoelectric structures. Int. J. Solids Struct. 42: 2399-2416.
- Hao, M., and Biao, W. 2004. T-stress in piezoelectric solid. Applied Mathematics and Mechanics 25.
- Hayami, K. 1992. A projection transformation method for nearly singular surface boundary element integrals. In: Brebbia CA, Orszag SA, editors. Lecture notes in engineering. Berlin: Springer-Verlag 73.
- Hayami, K., and Brebbia, C. A. 1988. Quadrature methods for singular and nearly singular integrals in 3-D boundary element method. In: Brebbia CA, editor. Boundary element X, vol. 1. Berlin: Springer-Verlag: 237-264.
- Hayami, K., and Matsumoto, H. 1994. A numerical quadrature for nearly singular boundary element integrals. Eng. Anal. Bound. Elem. 13: 143-154.

- Hou, P. F., Ding, H. J., and Guan, F. L. 2001. Point forces and point charge applied to a circular crack in a transversely isotropic piezoelectric space. Theoretical and Applied Fracture Mechanics 36: 245-262.
- Huang, Z., and Kuang, Z. B. 2003. A mixed electric boundary value problem for a two-dimensional piezoelectric crack. International Journal of Solids and Structures 40: 1433-1453.
- Hughes, T. J. R. 2000. The finite element method : Linear static and dynamic finite element analysis. Dover Publications, New York.
- Larsson, S. G., and Carlsson, A. J. 1973. Influence of non-singular stress terms and specimen geometry on small-scale yielding at crack tips in elastic-plastic materials. Journal of the Mechanics and Physics of Solids 21: 263-277.
- Lee, D. J., Shin, D. C., Cho, Y., and K., W. 2011. A study of the effect of the electro-mechanical loading history on the fracture strength of piezoelectric material. Engineering Fracture Mechanics 78: 1374-1388.
- Li, H. B., and Han, G. M. 1985. A new method for evaluating singular integrals in stress analysis of solids by the direct boundary element method. Int. J. Numer.Methods. Eng. 21: 2071-2098.
- Liu, S., Shen, Y., and Liu, J. 2012. Exact solutions for piezoelectric materials with an elliptic hole or a crack under uniform internal pressure. Chinese Journal of Mechanical Engineering 25: 845-852.
- Liu, Y., and Fan, H. 2001. On the conventional boundary integral formulation for piezoelectric solids with defects or of thin shapes. Eng. Anal. Bound. Elem. 25: 77-91.
- Martin, P. A., and Rizzo, F. J. 1996. Hypersingular integrals: how smooth must the density be? Int. J. Numer. Methhods Eng. 39: 687-704.
- Oden, J. T., and Carey, G. F. 1984. Finite elements Vol.V: Special problem in solid mechanics. Prentice Hall, New Jersey.
- Okayasu, M., Ozeki, G., and Mizuno, M. 2010. Fatigue failure characteristics of lead zirconate titanate piezoelectric ceramics. Journal of European Ceramic Society 30: 713-725.
- Pan, E. 1999. A BEM analysis of fracture mechanics in 2D anisotropic piezoelectric solids. Eng. Anal. Bound. Elem. 23: 67-76.
- Phongtinnaboot, W., Rungamornrat, J., and Chintanapakdee, C. 2011. Modeling of cracks in 3D piezoelectric finite media by weakly singular SGBEM. Engineering Analysis with Boundary Elements 35: 319-329.

- Qin, T. Y., and Noda, N. A. 2004. Application of hypersingular integral equation method to a three-dimensional crack in piezoelectric materials. JSME International Journal Series A 47(2): 173-180.
- Qin, T. Y., Y.S., Y., and Noda, N. A. 2007. Finite-part integral and boundary element method to solve three-dimensional crack problems in piezoelectric materials. Int. J. Solids Struct. 44: 4770-4783.
- Rajapakse, R. K. N. D., and Xu, X. L. 2001. Boundary element modeling of cracks in piezoelectric solids. Engineering Analysis with Boundary Elements 25: 771-781.
- Rungamornrat, J., and Mear, M. E. 2008a. Weakly-singular, weak-form integral equations for cracks in three-dimensional anisotropic media. International Journal of Solids and Structures 45: 1283-1301.
- Rungamornrat, J., and Mear, M. E. 2008b. A weakly-singular SGBEM for analysis of cracks in 3D anisotropic media. Computer Methods in Applied Mechanics and Engineering 197: 4319-4332.
- Rungamornrat, J., and Mear, M. E. 2008c. Analysis of fractures in 3D piezoelectric media by a weakly singular integral equation method. International Journal of Fracture 151: 1-27.
- Rungamornrat, J., and Senjuntichai, T. 2009. Regularized boundary integral representations for dislocations and cracks in smart media. Smart Materials and Structures 18.
- Sanz, J. A., M.P., A., and J., D. 2005. Three-dimensional BEM for piezoelectric fracture analysis. Eng. Anal. Bound. Elem. 29: 586-596.
- Shindo, Y., Narita, F., and Saito, F. 2007. Static fatigue behavior of cracked piezoelectric ceramics in three-point bending under electric fields. Journal of European Ceramic Society 27: 3135-3140.
- Solis, M., Sanz, J. A., Ariza, M. P., and Dominguez, J. 2009. Analysis of cracked piezoelectric solids by a mixed three-dimensional BE approach. Engineering Analysis with Boundary Elements 33: 271-282.
- Viola, E., Boldrini, C., and Tornabene, F. 2008. Non-singular term effect on the fracture quantities of a crack in a piezoelectric medium. Engineering Fracture Mechanics 75: 4542-4567.
- Wippler, K., and Kuna, M. 2007. Crack analyses in three-dimensional piezoelectric structures by the BEM. Comput. Mater. Sci. 39: 261-266.
- Xiao, L. 1998. Symmetric weak-form integral equation method for three-dimensional fracture analysis. Doctoral dissertation, The University of Texas at Austin.

- Xu, X. L., and Rajapakse, R. K. N. D. 1999. Analytical solution for an arbitrarily oriented void/crack and fracture of piezoceramics. Acta mater. 47: 1735-1747.
- Zhao, M. H., Fang, P. Z., and Shen, Y. P. 2004. Boundary integral–differential equations and boundary element method for interfacial cracks in three-dimensional piezoelectric media. Engineering Analysis with Boundary Elements 28: 753-762.
- Zhong, X. C., and Li, X. F. 2007. T-stress analysis for a Griffith crack in a magnetoelastic solid. Archive of Applied Mechanics 78: 117-125.
- Zhu, T., and Yang, W. 1999. Crack kinking in a piezoelectric solid. International Journal of Solids and Structures 36: 5013-5027.
- Zienkiewicz, O. C., and Taylor, R. L. 2000. The finite element method fifth edition volume 1: The basis. Butterworth-Heinemann, Oxford.

APPENDIX

By post-processing the complete generalized stress field given by Chen *et al.* (2000) using the series expansion procedure, the generalized T-stress for a penny-shaped crack in a transversely isotropic, linear piezoelectric, infinite domain under the uniformly distributed normal traction $t_3^+ = -t_3^- = \sigma_0$ and uniformly distributed surface elastic charge $t_4^+ = -t_4^- = d_0$ is given explicitly by

$$T_{11} = T_{33} = -\frac{\pi}{4} \left\{ 16\pi A \sum_{i=1}^3 p_i ((c_{66} - c_{11}) + c_{13} s_i \alpha_{i1} + e_{31} s_i \alpha_{i2}) \right\} \quad (\text{A.1})$$

$$T_{13} = T_{14} = T_{34} = 0 \quad (\text{A.2})$$

where all involved parameters are completely defined in Chen *et al.* (2000).

VITA

Tripop Subsathaphol was born on February 28, 1981 in Bangkok, Thailand, the son of Prasong Subsathaphol and Supa Subsathaphol. He graduated Bachelor of Engineering degree in Civil Engineering program from Mahanakorn University of Technology in 2011. In 2012, he decided to continue his study for Master's degree in Structural Engineering program at Chulalongkorn University. During this period he interest in fracture mechanic hence he decide to do the research under the supervision of Associate Professor Dr. Jaron Rungamornrat and Dr. Weeraporn Phongtinnaboot.

